



저작자표시-비영리-변경금지 2.0 대한민국

이용자는 아래의 조건을 따르는 경우에 한하여 자유롭게

- 이 저작물을 복제, 배포, 전송, 전시, 공연 및 방송할 수 있습니다.

다음과 같은 조건을 따라야 합니다:



저작자표시. 귀하는 원저작자를 표시하여야 합니다.



비영리. 귀하는 이 저작물을 영리 목적으로 이용할 수 없습니다.



변경금지. 귀하는 이 저작물을 개작, 변형 또는 가공할 수 없습니다.

- 귀하는, 이 저작물의 재이용이나 배포의 경우, 이 저작물에 적용된 이용허락조건을 명확하게 나타내어야 합니다.
- 저작권자로부터 별도의 허가를 받으면 이러한 조건들은 적용되지 않습니다.

저작권법에 따른 이용자의 권리는 위의 내용에 의하여 영향을 받지 않습니다.

이것은 [이용허락규약\(Legal Code\)](#)을 이해하기 쉽게 요약한 것입니다.

[Disclaimer](#)

Master's Thesis

Synergistic effect of lithium difluoro(bisoxalato)
phosphate and propionitrile for Li-ion batteries with
high discharge rate capability

Juyeon Lee

Department of Energy Engineering
(Battery Science and Technology)

Graduate School of UNIST

2020

Synergistic effect of lithium difluoro(bisoxalato)
phosphate and propionitrile for Li-ion batteries
with high discharge rate capability

Juyeon Lee

Department of Energy Engineering
(Battery Science and Technology)

Graduate School of UNIST

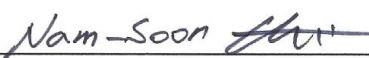
Synergistic effect of lithium difluoro(bisoxalato)
phosphate and propionitrile for Li-ion batteries
with high discharge rate capability

A thesis/dissertation
submitted to the Graduate School of UNIST
in partial fulfillment of the
requirements for the degree of
Master of Science

Juyeon Lee

12/10/2019

Approved by



Advisor

Nam-Soon Choi

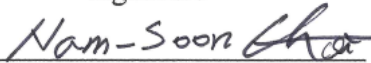
Synergistic effect of lithium difluoro(bisoxalato)
phosphate and propionitrile for Li-ion batteries
with high discharge rate capability

Juyeon Lee

This certifies that the thesis/dissertation of Juyeon Lee is approved.

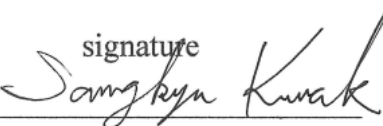
12/10/2019

signature



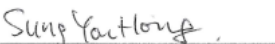
Advisor: Nam-Soon Choi

signature



typed name: Sang Kyu Kwak

signature



typed name: Sung You Hong

Abstract

Lithium-ion batteries (LIBs) have been widely used for various electronic devices from small electronics to power tools, electronic vehicles (EVs) and energy storage systems (ESS), taking advantages of their high capacity and efficiency featuring its lighter weight and higher energy density than the other batteries. Furthermore, the studies on LIB are working to broaden its application field as one of the leading candidates to resolve the environmental issues on greenhouse gas, typically CO₂ gas as well as due to its convenience. To expand the usage of LIBs, however, there are several issues to be overcome such as poor rate capability according to the effort to increase the energy density by using high-loading electrodes and so on.

In this study, propionitrile (PN, H₅C₂-CN) and lithium difluoro(bisoxalato) phosphate (LiDFBP) are introduced to enhance high discharge rate capability for LiNi_{0.8}Co_{0.1}Mn_{0.1}O₂ (NCM811) cathode and Si-containing graphite (Si-C) anode in lithium-ion batteries. The research reveals that the use of propionitrile as a cosolvent improved the mobility of lithium ions in the electrolyte. However, the irreversible capacity loss after the discharge rate test and the drastic decrease in the cycling test at high temperatures occur. To overcome this deterioration, LiDFBP as a lithium salt type electrolyte additive is adopted to form stable cathode-electrolyte interphase. Electrochemical tests proved that the LiDFBP effectively decreases the amounts of the byproduct of PN on the NCM811 cathode, improving the capacity recovery after discharge rate test and enabling the reversible cycling with capacity retention from 26.6% (LiDFBP-free PN) to 78.5% after 50 cycles at 0.5C rate at 45°C. The synergistic effect of PN cosolvent and LiDFBP additive is contact angle, XPS, SEM, and XRD analyses.

Contents

1. Introduction	
1.1 Lithium-ion batteries (LIBs)	
1.1.1 Demands for lithium-ion batteries (LIBs) -----	1
1.1.2 Problems of high-energy-density electrode materials: NCM and Si -----	3
1.1.3 Problems of high-mass-loading electrodes -----	5
1.2 Discharge rate capability	
1.2.1 Factors affecting discharge rate capability -----	7
1.2.2 Functional electrolyte design for discharge rate capability -----	9
2. Experimental	
2.1 Electrolytes and Electrodes -----	15
2.2 Electrochemical measurements -----	17
2.3 Characterization -----	18
3. Result and discussion	
3.1 Bulk characteristics of the electrolyte with PN cosolvent and LiDFBP additive -----	19
3.2 Effects of PN cosolvent and LiDFBP additive on the electrochemical performance -----	22
3.3 Surface Analysis -----	33
4. Conclusion -----	38
5. References -----	39

List of Figures

Figure 1. EV battery market trends by type and LIB ratio (2011-2020).

(Source: SNE Research, LIBs for EV applications: technology issues and market forecast (2011-2020), May 2013)

Figure 2. Schematic of a conventional lithium-ion battery.

Figure 3. Summarizing scheme of diverse issues for Ni-rich NCM with 1. high reactivity of Ni⁴⁺ 2. cation mixing and phase transition 3. microcracks.

Figure 4. Si electrode failure mechanisms: a) Material pulverization. (b) Change in morphology and volume. (c) Unstable SEI growth.

Figure 5. Discharge voltage curves depending on the electrode thicknesses at various C rates.

Figure 6. (a) Average discharge voltages at various cathode thickness; (b) A comparison of volumetric energy density in stack cell at various cathode thickness at the current rate of C/5, C/2, 1C, and 2C.

Figure 7. Schematic illustration showing the diffusion of Li-ion in the high-mass-loading electrode.

Figure 8. Schematic representation showing the diffusion of Li ions depending on using conventional carbonate electrolyte or the PFE cosolvent electrolyte in the dense electrodes.

Figure 9. Schematic representation showing a concentration gradient of Li-ion in the electrolyte at the start point of discharge.

Figure 10. Schematic illustration representing the effect of the FEC-derived SEI layer on rate capability.

Figure 11. long-term cycle test of Si@C electrode in the voltage range of 0.01 – 1.2V vs. Li/Li⁺ at various current densities with FEC or VC.

Figure 12. Schematic illustration explaining the positive effect of the LiDFBP additive by SEI formation on Li-rich cathode.

Figure 13. TGA of electrolytes containing solvents and lithium salts only, without additives such as VC, FEC, and LiDFBP.

Figure 14. A graph showing the viscosity and ionic conductivity of several electrolyte compositions at 25°C.

Figure 15. Photographs of electrolytes' contact angles on NCM cathodes and gra-SiC anodes.

Figure 16. Floating test of NCM/Li half cells charged to 4.3V at C/10 rate and 25°C, magnified to show normalized leakage currents.

Figure 17. Transition metal dissolution degree analyzed by inductively coupled plasma (ICP).

Charged cathodes with Carbonate w/o additive were stored in (a) Carbonate electrolyte and (b) Nitrile electrolyte. (c) Charged cathode with Nitrile and (d) pristine cathode were stored in Nitrile w/o additive.

Figure 18. Illustration of TM dissolution of Nitrile out of the NCM cathode.

Figure 19. Density functional theory (DFT) calculation of HOMO-LUMO energy level and chemical structures. (EC, FEC, and LiDFBP in neutral charge of the molecule. C, H, O and F atoms are represented in gray, white, red and cyan colored spheres, respectively.)

Figure 20. (a) Charge-discharge curves and (b) charge differential capacity (dQ/dV) plots on the NCM/gra-SiC full cells during precycle under C/10 at 25°C.

Figure 21. (a) Comparison of the discharge rate capability of NCM/gra-SiC full cells with electrolytes whether containing nitrile cosolvent and LiDFBP additive or not. The discharge rate was from C/2 to 2C with the fixed C/2 charge rate. (b) The AC impedance spectra of NCM/gra-SiC full cells after the precycle.

Figure 22. XRD patterns of the gra-SiC anodes in the electrolyte with and without propionitrile and LiDFBP.

Figure 23. (a) Cycle retention and (b) coulombic efficiency of NCM/gra-SiC full cells in the voltage range 2.5 – 4.2 V at a rate of C/5 at 45 °C.

Figure 24. BSE images from the cross-sectional SEM of NCM cathodes (a), (b) pristine, (c), (d), (g) cycled using Nitrile electrolyte, and (e), (f), (h) cycled using Nitrile + LiDFBP electrolyte.

Figure 25. BSE images from the cross-sectional SEM of gra-SiC anodes (a), (c) cycled with Nitrile electrolyte, and (b), (d) cycled with Nitrile + LiDFBP electrolyte.

Figure 26. F 1s, O 1s and N 1s XPS spectra of the NCM cathodes retrieved from NCM/gra-SiC full cells (a), (c), (e) after precycle and (b), (d), (f) after the cycle test.

Figure 27. (a) Cobalt atom's charge change depending on the bulk and the surface after delithiation. (b) The effective charge of cobalt versus cobalt-succinonitrile complex depending on in the bulk or at the surface.

Figure 28. F 1s, P 2p, and N 1s XPS spectra of gra-SiC anodes from NCM/gra-SiC full cells (a), (c), (e) after precycle at C/10 and 3 cycles at C/2 and 25°C, and (b), (d), (f) after 50 cycles at C/2 and 45°C.

List of Tables

Table 1. Candidates for solvent with low viscosity (LUMO and HOMO value calculated by Gaussian 09)

Table 2. Composition of electrolytes.

1. Introduction

1.1 Lithium-ion batteries (LIBs)

1.1.1 Demands for lithium-ion batteries (LIBs)

Rechargeable batteries have been vigorously studied to keep up with the development of mobile electronics and to solve the environmental issues on reducing CO₂ gas emission.[1], [2] Among them, LIB has been developed as the most feasible candidate for its high operating voltage (average 3.6-3.7V), high energy density, and low self-discharge rate without memory effect.[1], [3] Moreover, the LIBs are broadening their application field from small portable electric devices to electronic vehicles (EVs).[4] In particular, the EV market estimated by SNE Research indicates increasing demands for LIBs for application in EV. (**Figure 1**)

The working principle of a conventional LIB is shown in **Figure 2**. During the charging process, lithium ions diffuse from a lithiated cathode to a delithiated anode with accompanying oxidation and reduction of the two electrodes, respectively. Surface film formation occurs on anode and cathode, named as solid electrolyte interphase (SEI) layer and cathode solid electrolyte interphase (CEI) layer. The reverse process occurs during discharge.[2] A LIB consists of cathode (e.g. LiCoO₂), anode (e.g. graphite), separator and non-aqueous electrolyte including lithium salts (e.g. LiPF₆) in a mixture of organic solvents. The cathode material is the source of lithium ions, which decides the capacity and operating voltage of batteries. The anode material stores the lithium ions from the cathode and releases them generating electricity. The separators are a physical barrier preventing the electrical short. The role of electrolytes is to mediate the transportation of Li ions through immigration of solvated Li ions from the cathode to anode during charging and in reverse direction during discharging. The electrolytes are comprised of organic solvents, lithium salts, and additives. At present, however, state-of-the-art LIBs, with a specific energy of ~150 WH/kg, do not yet have enough energy or life for using in EV.[5] For the need of much superior energy and power densities, several strategies on research and development have continued in the development of improved materials.²

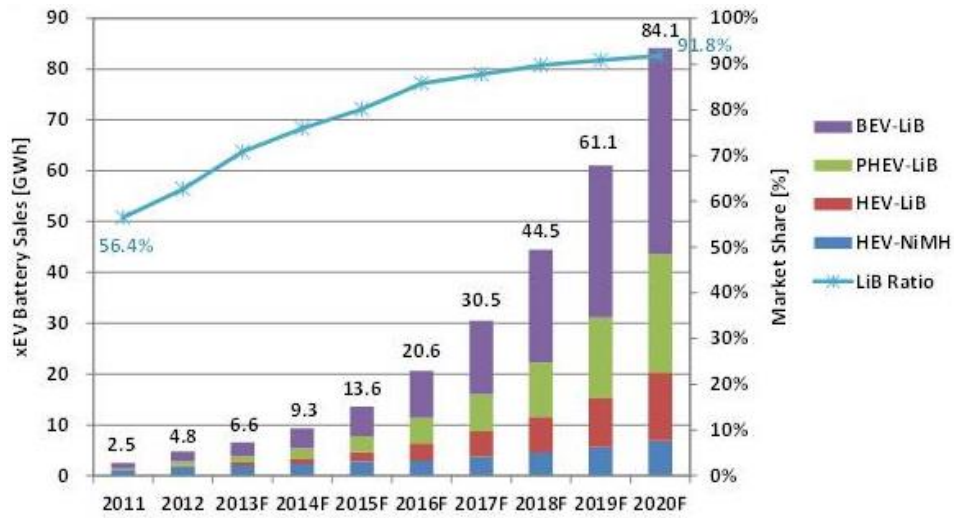


Figure 1. EV battery market trends by type and LIB ratio (2011-2020).

(Source: SNE Research, LIBs for EV applications: technology issues and market forecast (2011-2020), May 2013)

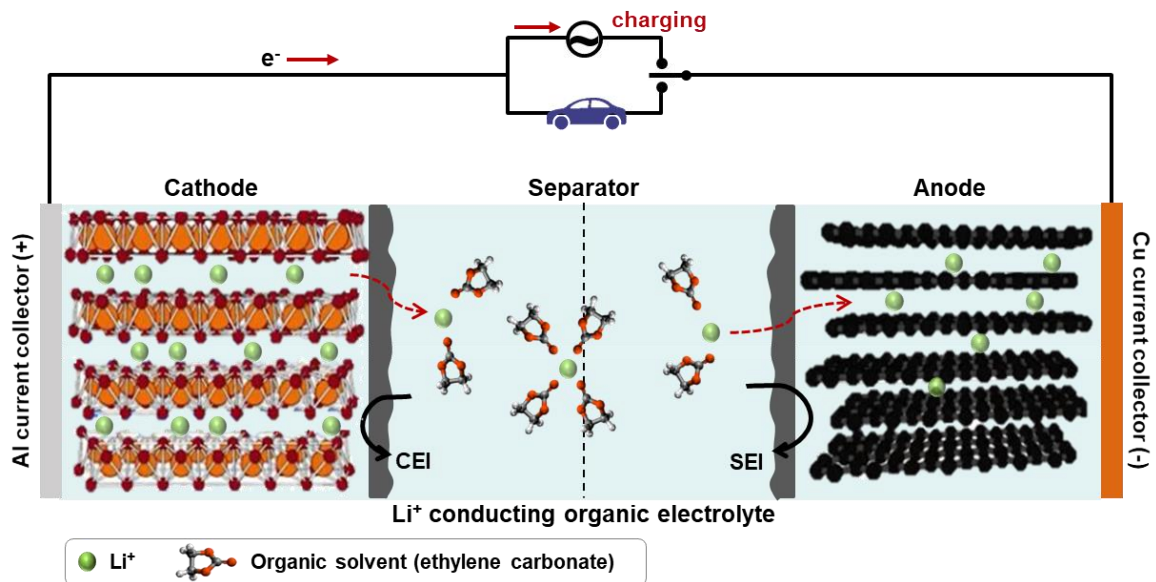


Figure 2. Schematic illustration of a conventional lithium-ion battery.

1.1.2 Problems of high-energy-density electrode materials: NCM and Si

There have been several approaches to improve the performances of LIBs through the development of new materials in LIBs.[5] For the high-energy-density LIBs, the new active materials with high theoretical capacity such as Ni-rich cathode and silicon anode have been researched.⁶⁻⁸

The Ni-rich cathode, commonly called NCM (e.g. NCM811 for $\text{LiNi}_{0.8}\text{Co}_{0.1}\text{Mn}_{0.1}\text{O}_2$), has higher capacity, rate capability, and safety in the role of nickel, cobalt, and manganese respectively than other single transition metal-containing cathodes such as LiCoO_2 , LiNiO_2 , and LiMnO_2 . [6] As the Ni contents increased for high energy density, however, several problems are hindering the advantages of Ni-rich NCM. The high reactivity of Ni^{4+} , phase transition by cation mixing and formation of microcracks in secondary particles, as shown in **Figure 3**. [6]

The silicon is one of the promising anode materials in that the theoretical capacity is ten times higher than graphite (~ 4200 mAh/g for $\text{Li}_{4.4}\text{Si}$ versus 372 mAh/g for LiC_6). Unfortunately, the severe volume expansion occurs due to the alloy reaction during lithiation and delithiation, which results in particle pulverization, unstable SEI layer, and electrical disconnection, as illustrated in **Figure 4**. [8]

The deterioration of the active electrode materials can result in poor electrochemical performances like capacity fading and limited cycle life. [6]–[8]

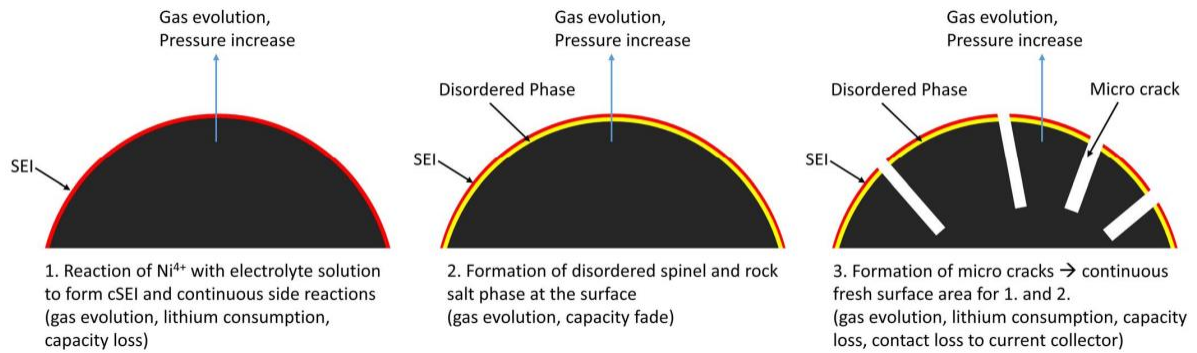


Figure 3. Summarizing scheme of diverse issues for Ni-rich NCM with 1. high reactivity of Ni^{4+} 2. cation mixing and phase transition 3. microcracks.

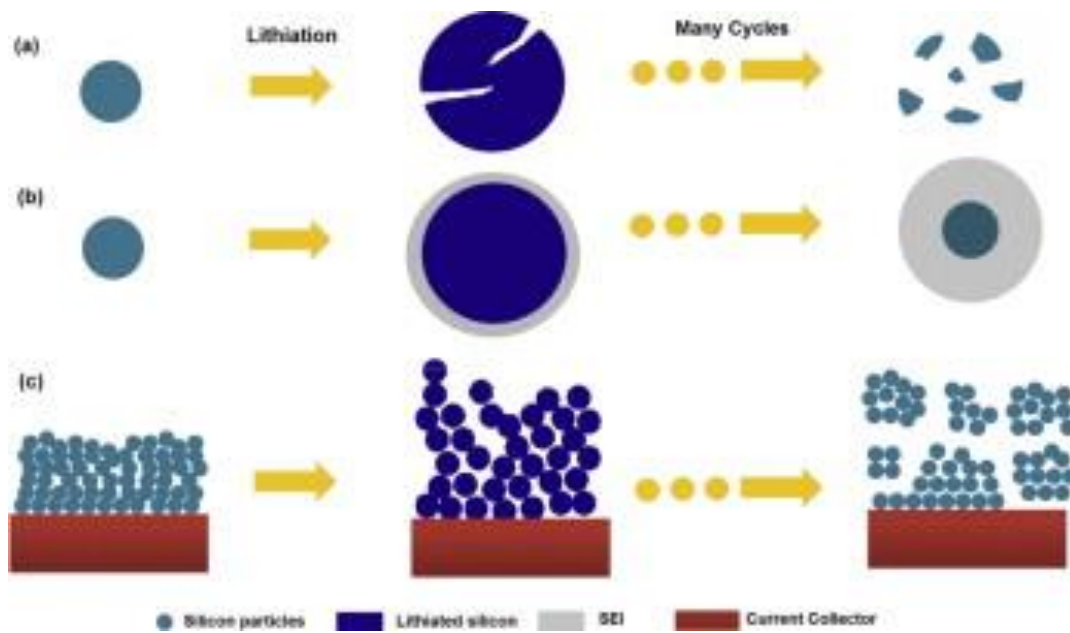


Figure 4. Si electrode failure mechanisms: a) Material pulverization. (b) Change in morphology and volume. (c) Unstable SEI growth.

1.1.3 Problems of high-mass-loading electrodes

Another effective strategy for the development of high-energy-density LIBs is increasing the volume ratio of active materials by increasing electrode thickness. [9] However, the corresponding problems on the application of batteries as followed.

The high-mass-loading electrodes cause degradation of the rate capability of batteries. **Figure 5** shows the discharge voltage curves versus the capacity in $C/5$, $C/2$, $1C$, and $2C$ rates. The initial discharge capacity remained the same regardless of increasing electrode thickness at $C/5$. In contrast, it dramatically declined as the C rates increases. Another sensitive factor is the average discharge voltage. (**Figure 6**) The polarization of the cell rapidly increases depending on the electrode thickness when the applied current is increased, while one at $C/5$ rate is almost constant regardless of the thickness of electrodes. The decrease of capacity and cell voltage due to the polarization result in decreased energy and power density, canceling out the advantage from the high mass loading in the thick electrode.[9]

Therefore, finding strategies to maintain the energy density without a sacrifice of power density is vital for the high-mass-loading electrode.

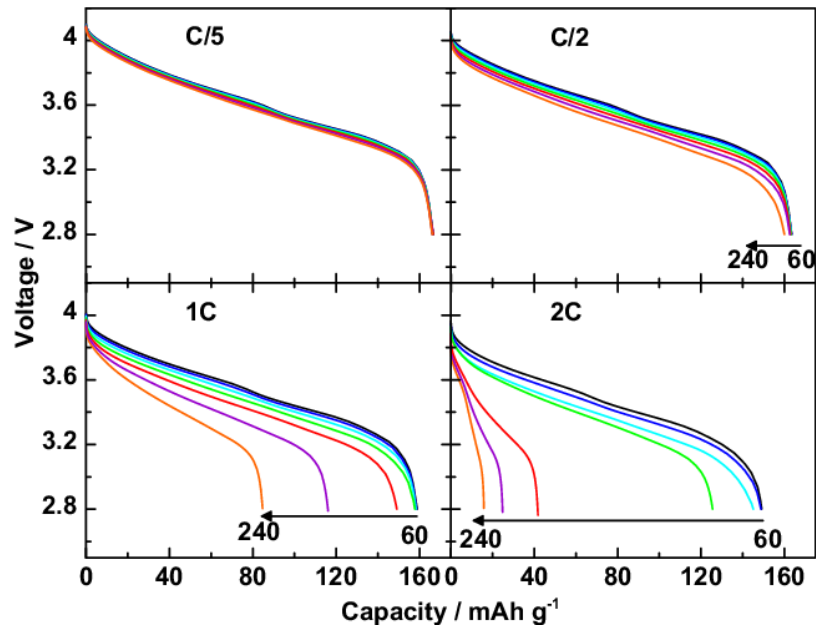


Figure 5. Discharge voltage curves depending on the electrode thicknesses at various C rates.

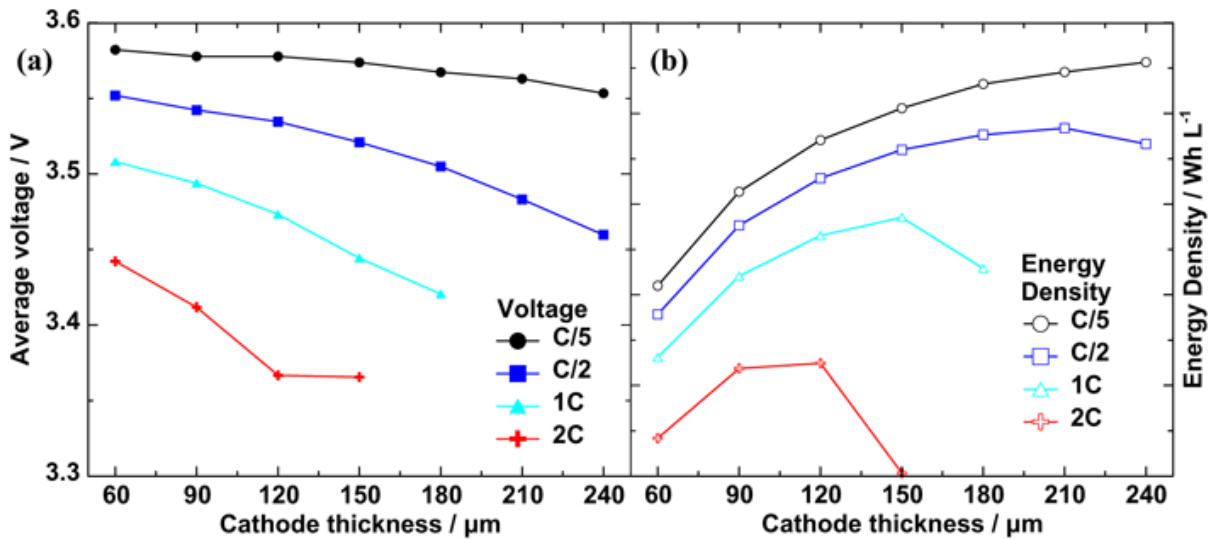


Figure 6. (a) Average discharge voltages at various cathode thickness; (b) A comparison of volumetric energy density in stack cell at various cathode thickness at the current rate of C/5, C/2, 1C, and 2C rates.

1.2 Discharge rate capability

1.2.1 Factors affecting rate capability of high-mass-loading electrode

Zheng et al examined that the rate-determining step for the discharge process is Li-ion diffusion within the electrode. [10] The long diffusion path through the thick and tortuous electrode leads to the low diffusion rate of Li ions and slower Li-ion kinetics. [9]–[12] The inferior Li-ion diffusion inside the electrode augments cell polarization (IR drop) and underutilization of active materials. (**Figure 7**) One promising method to enhance Li-ion diffusion is introducing the electrolyte with low viscosity and high impregnation characteristic, which can faster the Li-ion diffusion rate and the permeation characteristic of electrolytes through inner pores of electrodes, utilizing entire active materials and relieving the IR drops. [9], [13] Choi et al. reported a low viscosity electrolyte using partially fluorinated ether and fluoroethylene carbonate for solvents. [13] **Figure 8** shows the facile Li-ion diffusion with PFE-containing electrolyte by improved wettability and maximized mobility of Li-ion through the inner pores inside the electrode.

Furthermore, the active materials undergo rapid volume change during charging and discharging processes in a high current density. The expansion and contraction of the active material particles accumulate intense stress within the thick electrode because the internal stress is hard to release compared to the thin electrode. [10] The additive in the electrolyte can resolve this problem, forming a flexible and stable SEI layer to endure the volume expansion. [14]

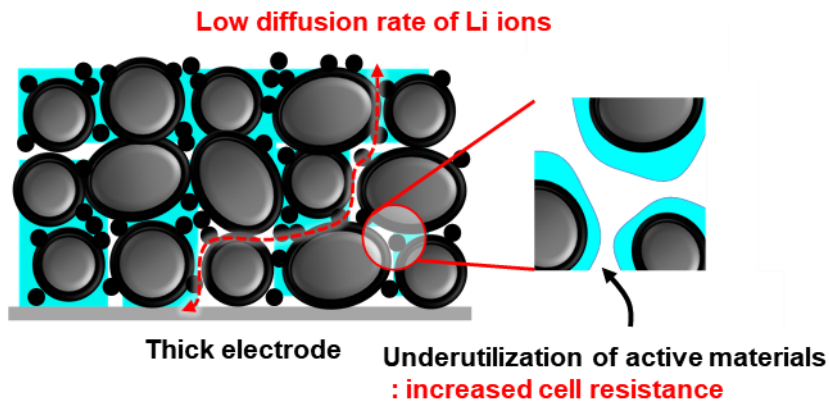


Figure 7. Schematic illustration showing the diffusion of Li-ion in high-mass-loading electrode.

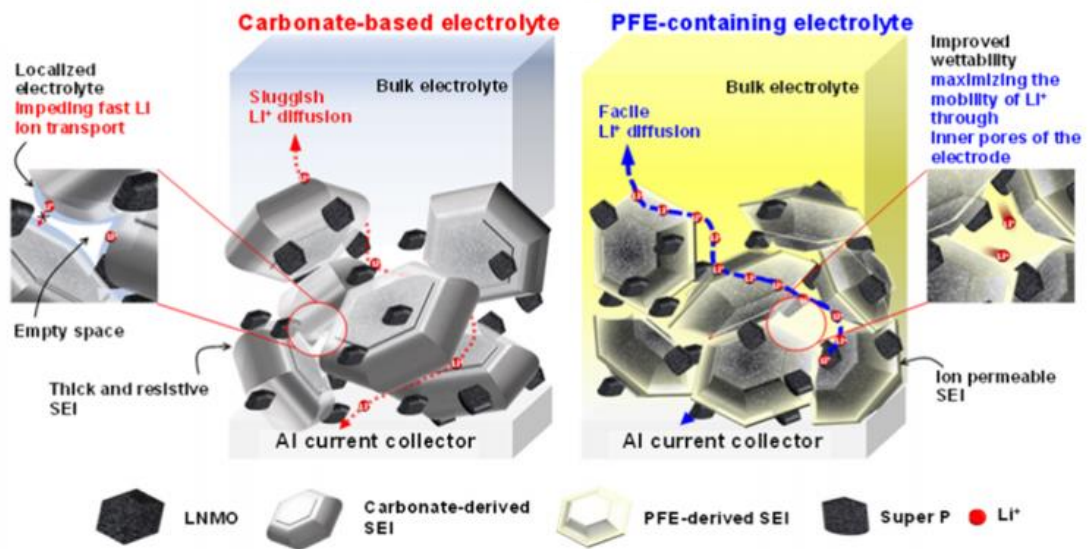


Figure 8. Schematic representation showing the diffusion of Li ions depending on using conventional carbonate electrolyte or the PFE cosolvent electrolyte in the dense electrodes.

1.2.2 Functional electrolyte design for discharge rate capability

Figure 9 shows the Li-ions inside the battery when starting fast discharging. The Li-ion transport process is followed by this order; delithiation from the anode, transport through SEI, solvation by organic solvents, diffusion in the form of a solvent sheath, desolvation at the cathode surface, transport through CEI and finally diffusion inside the cathode. Thus, the proper functions of electrolytes are required for each step. In the point of electrolyte material, the selection of the components is critical such as low viscosity solvent and appropriate additives. In this study propionitrile (PN) cosolvent and vinylene carbonate (VC), fluoroethylene carbonate (FEC) and lithium difluoro(bisoxalato) phosphate (LiDFBP) were adopted for discharge rate capability. The procedure of selection follows the next paragraph.

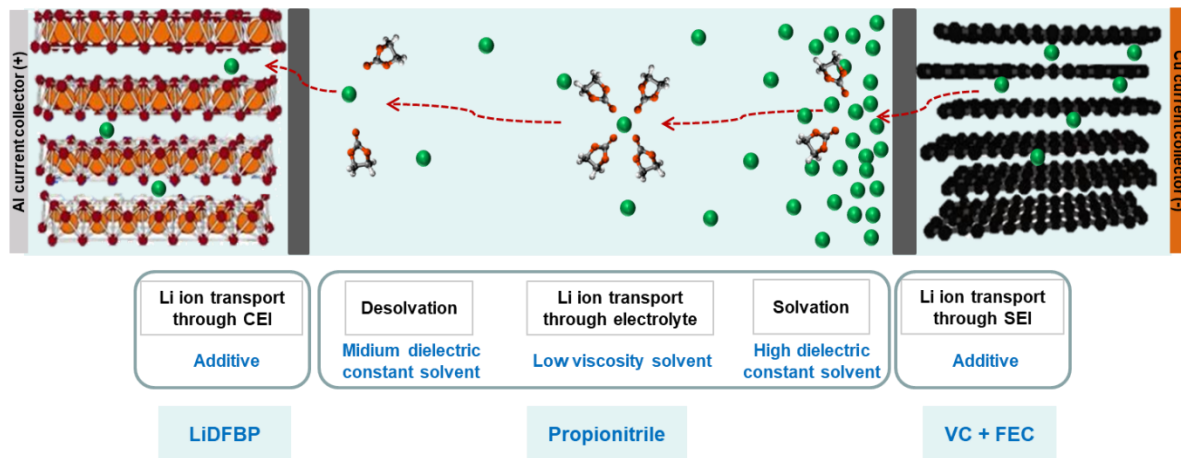


Figure 9. Schematic representation showing a concentration gradient of Li-ion in the electrolyte at the start point of discharge.

For the low viscosity electrolyte, the selection of solvent comprising most of the electrolyte is the most important step. Several solvent candidates are listed in Table **Table 1**. The solvent generally requires two kinds of ability; dissolution of lithium salt-forming solvation sheath and desolvating Li-ions and presenting high ionic conductivity. The dielectric constant of the solvent has a huge amount of influence on the dissociation and association of Li ions. The higher dielectric constant a solvent has, the more lithium salts experience dissociation since the dielectric constant is in inverse proportion to the coulombic force between cations and anions comprising lithium salt. However, the ionic conductivity decreases as the viscosity increases with increasing polarity due to the high dielectric constant. To balance between the dielectric constant and ionic conductivity values, cyclic carbonate (e.g. ethylene carbonate (EC)) and linear carbonate (e.g. diethyl carbonate (DEC)) have been widely used targeting for high Li-ion dissociation feature and low viscosity feature, respectively. Besides, there are several factors for the decision of solvents, for example, high boiling point, low melting point, and a wide electrochemical window.

Dimethyl carbonate (DMC) is a typically utilized carbonate solvent for fast Li-ion diffusion. However, it has a fatal disadvantage of high volatility because of the low boiling point, postponing the application for pouch cells. From the boiling point view, dimethoxyethane (DME) and methyl propionate (MP) show lower b.p. than DMC. Another considering factor is the stability of oxidation and reduction with the highest occupied molecular orbital (HOMO) and lowest unoccupied molecular orbital (LUMO). The DME has high HOMO indicating low anodic stability. Concerning the viscosity of the solvent, ethyl propionate (EP) and butyronitrile (BN) are excluded owing to relatively high viscosity. Therefore, propionitrile (PN) has been chosen for the cosolvent with existing carbonate solvent like EC and ethyl methyl carbonate (EMC). PN has advantages on the high dissociation capability with high dielectric constant without concern of viscosity being depleted, low volatility, and high anodic stability.

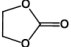
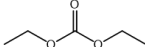
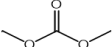
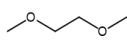
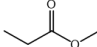
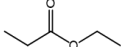
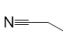
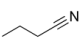
	Ethylene carbonate (EC)	Diethyl carbonate (DEC)	Dimethyl carbonate (DMC)	Dimethoxyethane (DME)	Methyl propionate (MP)	Ethyl propionate (EP)	Propionitrile (PN)	Butyronitrile (BN)
Structure								
Molecular weight (g/mol)	88.06	118.13	90.00	90.12	88.11	102.13	55.08	69.11
Melting point (°C)	40	-43	3	-58	-88	-73	-93	-112
Boiling point (°C)	248	126.8	90	85	80	99	97	117
Viscosity (cP, 25 °C)	1.9 (40°C)	0.75	0.59	0.46	0.43	0.51	0.41	0.55
LUMO (eV)	-0.35	-0.10	0.08	0.24	-0.21	-0.15	-0.34	-0.24
HOMO (eV)	-8.60	-7.97	-8.07	-7.03	-7.76	-7.67	-9.45	-9.24
Dielectric constant (25 °C)	90	2.8	3.2	7.2	6.2	5.7 (20°C)	27.7	20.7

Table 1. Candidates for solvent with low viscosity (LUMO and HOMO value calculated by Gaussian 09).

Besides, the functionalized SEI layer could assist the rate capability of the batteries by the protection of the electrode surface and formation of the ion-permeable SEI layer. [15]–[17]

VC and FEC additives are the most popular additives to reductive decomposition at the anode surface. [15] VC and FEC forming SEI layer on the anode surface consist of a polymeric film to suppress electrolyte decomposition. [14], [18], [19], [20] In VC containing electrolytes, the presence of double bonds in VC structure leads to faster reduction than other carbonate solvents and forms polycarbonate components named in poly(VC). [20] FEC goes through decomposition to VC by defluorination, generating HF to form polycarbonate species like VC as well. [14] Furthermore, FEC can support the fast kinetic of Li-ion across grain boundaries such as Li_2CO_3 , LiF and $\text{R-OCO}_2\text{Li}$. [17] In terms of the cycle performance, in contrast, the VC additive outperforms the FEC additive due to the formation of the very flexible polymeric protective film which can endure the volume changes during cycles. **(Figure 10)**

The stable polycarbonates formed by VC reduction contribute to the thermal stability of the battery and suppress additional electrolyte decomposition. In contrast, the FEC forms a less flexible and less reversible SEI layer compared to VC, but rich in LiF species can improve the rate capability. [15] Therefore, the performance of the battery can be enhanced by the synergistic effect of using a mixture of VC and FEC as an SEI layer forming additives. [5] **(Figure 11)**

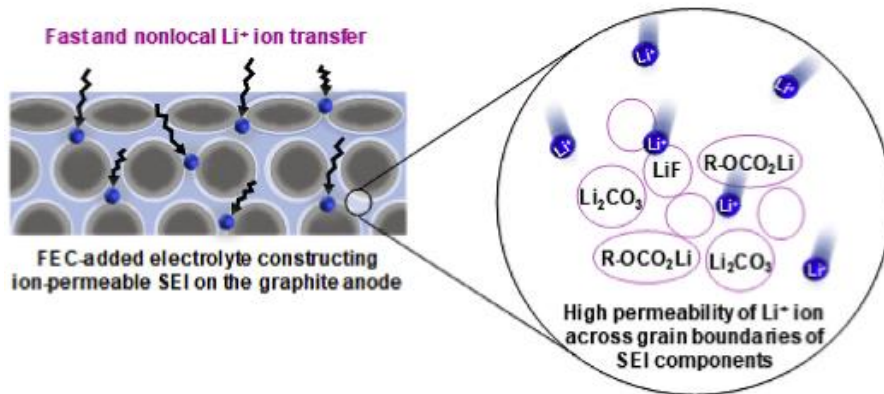


Figure 10. Schematic illustration representing the effect of the FEC-derived SEI layer on rate capability.

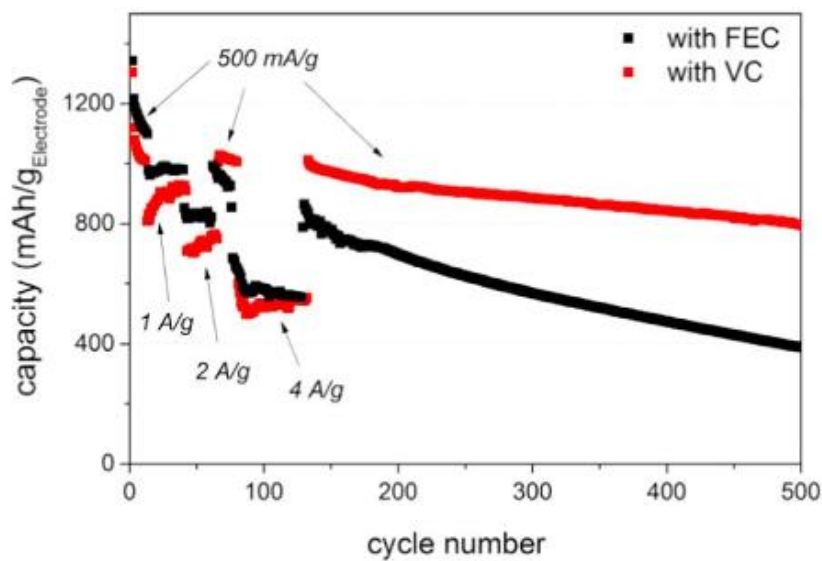


Figure 11. long-term cycle test of Si@C electrode in the voltage range of 0.01 – 1.2V vs. Li/Li^+ at various current densities with FEC or VC.

Modification of the cathode surface could be another strategy for rate capability. Various approaches were using phosphorous-containing additives, HF scavenging additive, lithium salt type additive and so on. Among them, lithium difluoro(bisoxalato) phosphate was reported by Choi et al. The LiDFBP is one of the lithium salt type additives, which prevents electrolyte decomposition on the cathode by stable CEI layer formation by oxidation as shown in **Figure 12**. [16]

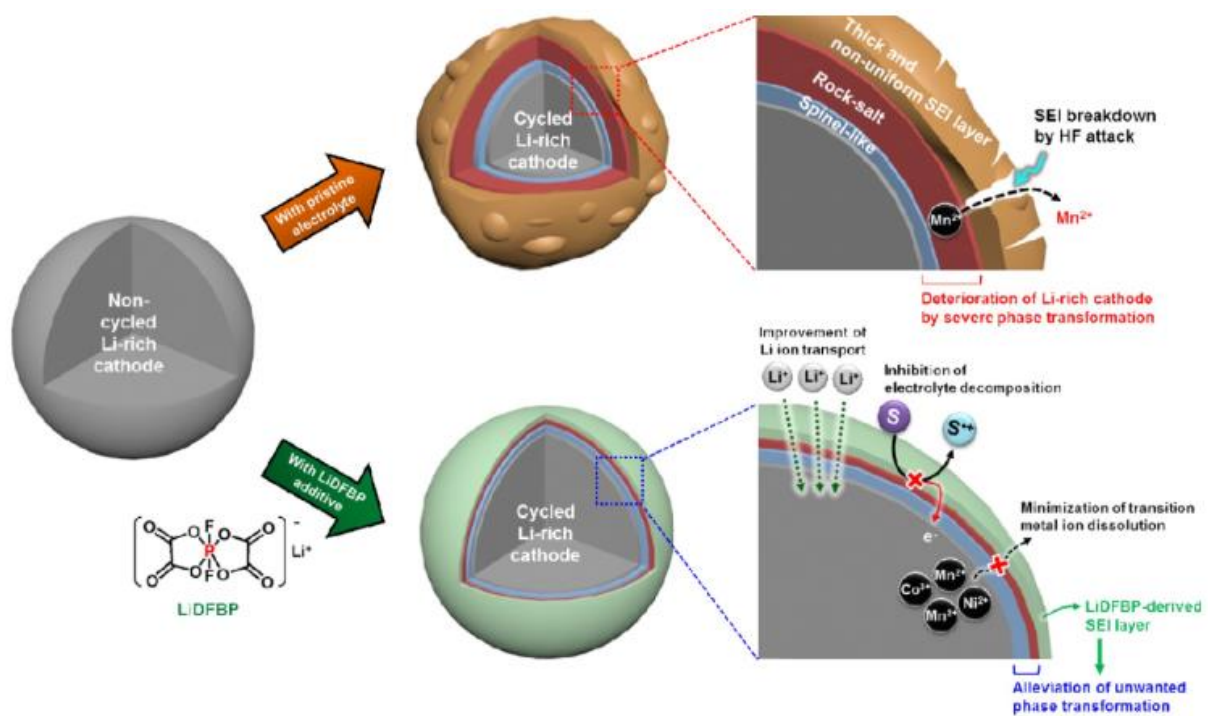


Figure 12. Schematic illustration explaining the positive effects of the LiDFBP additive by SEI formation on Li-rich cathode.

2. Experimental

2.1 Electrolytes and Electrodes

Four different compositions of electrolytes were used, as shown in **Table 2**. They contain the battery-grade lithium salt, solvents, and additives. The lithium salt is lithium hexafluorophosphate (LiPF_6 , 99.9%, Soul brain). The solvent consists of ethylene carbonate (EC, 99.9%, Soul brain), ethyl methyl carbonate (EMC, 99.9%, Soul brain) and diethyl carbonate (DEC, 99.9%, Soul brain) or propionitrile (PN, 99%, Sigma-Aldrich) with 25:45:30 volume ratio. Vinyl carbonate (VC, Enchem Co., Ltd) and fluoroethylene carbonate (FEC, Enchem Co., Ltd) were used as additives to form an effective SEI layer on the anodes. Moreover, lithium difluoro(bisoxalato) phosphate (LiDFBP, Chunbo) were included as an additive in Carbonate + LiDFBP and Nitrile + LiDFBP. H_2O impurity in every solvent mixture was treated by Calcium hydride (CaH_2 , Sigma-Aldrich) twice before LiPF_6 salt was added and after all, components were mixed. The moisture ratio was confirmed less than 10ppm through measurement by Karl Fischer titrator (C30, Mettler Toledo) except for PN. PN contains approximately 407 ppm of H_2O according to the Karl Fischer titrator. It decreased to 273 ppm after reaction with CaH_2 and to 47 ppm even after mixed with other solvents and reacted with CaH_2 . The final electrolyte with every component was confirmed to include less than 10 ppm of moisture.

Code	Composition
Carbonate	1M LiPF_6 in EC/EMC/DEC (25/45/30 vol%) + 1% VC + 3% FEC
Carbonate + LiDFBP	Carbonate + 1.5 wt% LiDFBP
Nitrile	1M LiPF_6 in EC/EMC/PN (25/45/30 vol%) + 1% VC + 3% FEC
Nitrile + LiDFBP	Nitrile + 1.5 wt% LiDFBP

Table 2. Composition of electrolytes.

For electrochemical tests, NCM cathode and SiC containing graphite anode were used for the 2032 coin full cells. The cathode was comprised of $\text{Li}[\text{Ni}_{0.8}\text{Co}_{0.1}\text{Mn}_{0.1}]\text{O}_2$ (NCM, mixed with large and small particles) and other compounds like conductors and binders dissolved in N-methyl-2-pyrrolidone (NMP). The mixture of SiC and graphite as active materials (gra-SiC), other conducting materials and binders were used as the anode. The detailed components and ratios are not allowed. The mass loading of cathode and anode were 21.9 mg/cm^2 and 10.9 mg/cm^2 , respectively. The separator was a polyethylene membrane coated by Al_2O_3 (PE, classified). The thickness was $15.1 \mu\text{m}$ and porosity was 49.2%.

2.2 Electrochemical tests

2032 coin type full cell of NCM/gra-SiC was manufactured in a glove box filled with argon under control of H₂O and O₂ less than 1.0 ppm. The formation cycle was performed at C/10 rate between 2.5-4.2V at 25°C, and the constant-voltage (CV) mode was applied at 4.2V before discharging step until the current decrease to C/20 (WonATech WBCS 3000). The stability of electrolyte on the cathode was examined by a floating test at 25°C, in which 2032 coin type NCM/Li half cells were charged to 4.3V in a C/10 rate and 4.3V was applied for 6 hours at a constant voltage mode. The NCM cathode in the half cell was fabricated with a low loading level of 10.2mg/cm² to avoid the polarization when charging. For the rate capability test confirming the effect of propionitrile and LiDFBP on rate capability, the full cells were tested with a various discharge rate of C/2, 1C, 1.5C and 2C and a fixed charge rate of C/2 for 3 cycles at each C rates at 25°C. The cycle test at elevated temperature was performed at 45°C, with C/2 from 2.5-4.2V.

2.3 Characterization

For thermogravimetric analysis (TGA) of the electrolytes, a TGA Q500 (TA Instruments) was used. Each sample was heated from room temperature to 300°C with a heating rate of 5 K/min.

Oakton CON 11 standard conductivity meter and BROOKFIELD viscometer (LVDV-II+P) were utilized to measure the ionic conductivity and viscosity of an electrolyte.

The wetting ability of electrolytes was examined by contact angle measurements on the NCM cathode and gra-SiC anode using a Phoenix 300 and a 10 μ L electrolyte was dropped to photograph all snapshots after dropping within 2 s.

The inductively coupled plasma (ICP-OES) analysis was carried out on 700-ES Varian. A retrieved cathode rinsed with DMC solvent after precycle and additional charge or a pristine cathode was stored in 2 g of electrolyte to confirm the transition metal dissolution contents by the interaction of cathode and electrolyte

To examine the electrochemical window of the organic solvent and additives, the molecule optimization of geometry was obtained using density functional theory with Gaussian 09 at the B3LYP/6-311+G level.

After two formation cycles, the electrochemical impedance spectroscopy (EIS) measurements for full cells were carried out using an IVIUM frequency response analyzer. The frequency range was from 10mHz to 1MHz and the potentiostat signal amplitude was 5mV.

For the analysis of electrodes after electrochemical tests, the full cells were cautiously separated in a glove box. Dimethyl carbonate (DMC) rinsing was carried out to remove the residual electrolyte on the electrodes and they were dried at room temperature. The *ex-situ* X-ray photoelectron spectroscopy (XPS, Thermo Fisher) measurements were conducted to investigate the surface compositions with Al K α ($h\nu = 1486.6$ eV) radiation in an ultrahigh vacuum environment. XPS spectrum was gathered in a 0.10 eV step size and 50 eV passing energy. The hydrocarbon peak at 285 eV was the baseline for all XPS spectra.

The crystal structure of the delithiated anode was investigated after 2C rate discharge cycles on the rate capability test by the X-ray diffraction (XRD). Bruker D2 Phaser powder diffractometer with a Cu K α radiation source ($\lambda = 1.54184$ Å) was used. The scanning 2θ range was 23-27° at 1°/min.

After the cycle test at 45°C, the degradation of the NCM cathode was observed through a field-emission scanning electron microscope (FE-SEM, JEOL, JSM-6700F) under vacuum condition. The cross-sections of the electrodes were obtained using ion milling (HITACHI IM4000) carried with argon⁺ ions at beam angles ranging between 0° and 60° from normal incidence.

3. Result and discussion

3.1 Bulk characteristics of electrolytes containing PN and LiDFBP

To ensure the thermal stability of PN cosolvent, the TGA of the electrolytes containing lithium salt and solvent mixture without any additives were performed, as shown in **Figure 13**. The evaporation time takes longer for the Nitrile w/o additive. It shows relatively higher thermal stability and decreased volatility than the carbonate-based electrolyte, thanks to the high boiling point of the PN, suppressing the vaporization of the electrolyte.

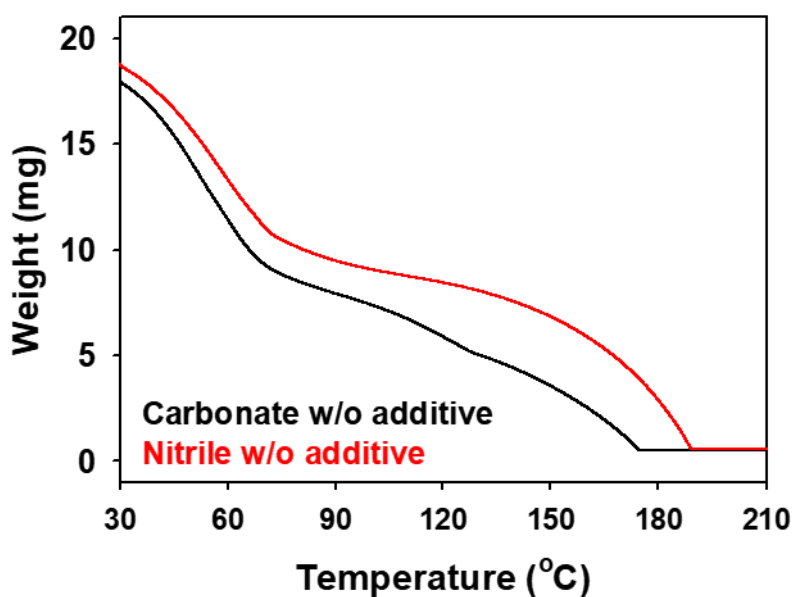


Figure 13. TGA of electrolytes containing solvents and lithium salts only, without additives such as VC, FEC, and LiDFBP.

The ionic conductivity and viscosity were measured to examine the effect of PN cosolvent and LiDFBP additive for the bulk characteristics of electrolyte. (**Figure 14**) The ionic conductivity dramatically increases when propionitrile was introduced as a cosolvent. The high ionic conductivity originates from the high dielectric constant (27.7 at 25°C) and low viscosity of propionitrile (0.41 cP at 25°C). However, the LiDFBP additive slightly decreases the ionic conductivity because of the heavy weight. This indicates that the electrolytes with the propionitrile will show improved rate capability.

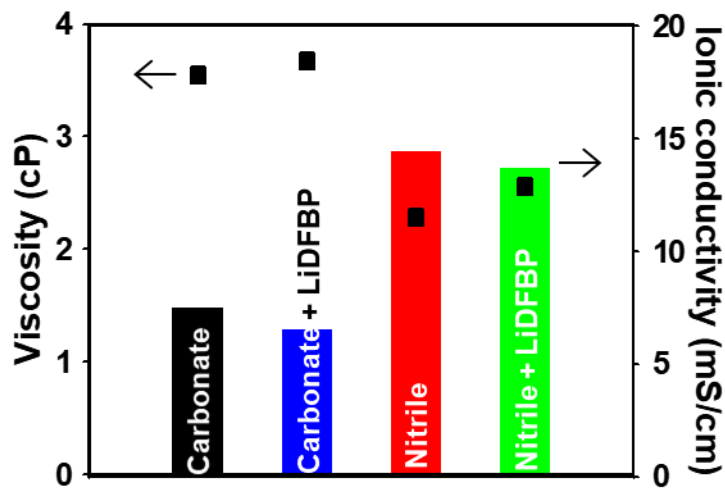


Figure 14. A graph showing the viscosity and ionic conductivity of several electrolyte compositions at 25°C.

The impregnation characteristic of electrolytes toward electrodes is also regarded as another important factor for improving the electrochemical kinetics of electrodes. The contact angle measurement was conducted to examine the impregnation characteristic of the electrolytes on the high-mass-loading NCM cathode, as shown in **Figure 15**. The Nitrile electrolyte showed a much lower contact angle than Carbonate electrolyte, which indicates the better wettability toward the high-mass-loading NCM cathode. The Nitrile electrolyte revealed the improved wetting property on the gra-SiC anode than the carbonate electrolyte as well. The contact angles of electrolytes with LiDFBP additive were slightly larger than without LiDFBP because of the higher viscosity. From this result, Nitrile supported by its low viscosity was demonstrated to have improved the impregnation characteristic of electrolytes toward the high-mass-loading electrode. [21], [22]

Therefore, the low viscosity and the improved impregnation characteristic of PN cosolvent showed the possibility of enhancing the rate capability performance of full cells, complementing the drawback of thick electrodes.

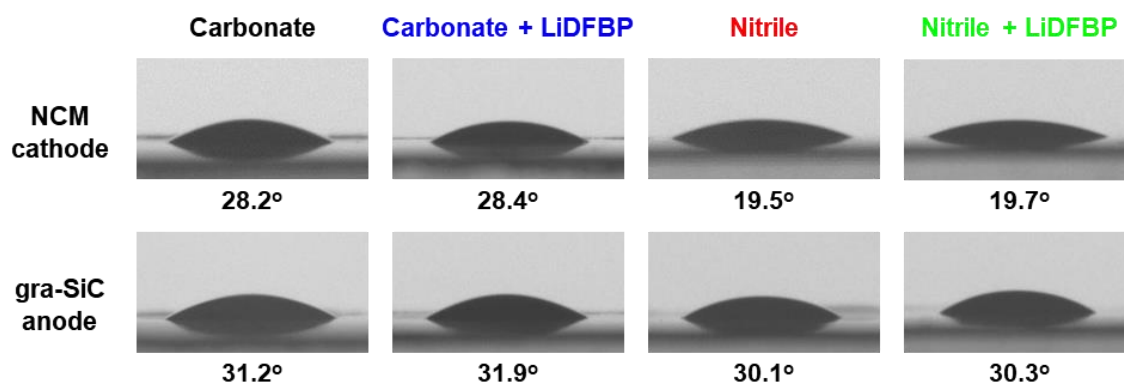


Figure 15. Photographs of electrolytes' contact angles on NCM cathodes and gra-SiC anodes.

3.2 Effects of PN cosolvent and LiDFBP additive on the electrochemical performance

The electrochemical floating test was carried out for confirmation of the voltage stability of PN cosolvent on the NCM cathode. **(Figure 16)** The Nitrile electrolyte showed higher oxidation current, which implies the instability of the Nitrile toward the NCM cathode, which is the opposite result to the calculated HOMO of PN indicates the stability of oxidation. This contradiction is supposed to be derived from the reactivity of PN with the NCM cathode. The high instability of propionitrile towards the NCM cathode material was revealed in **Figure 17**. The result from test samples of A and B convinces the transition metal (TM) dissolution tendency of Nitrile electrolyte. The Nitrile shows a much higher content of TM after storage in 60°C for 1 day. Furthermore, the test sample C and D was stored to figure out whether the PN has a chemical interaction with TM ions in cathode without any electric force. The charged cathode containing reactive TM ions such as Ni³⁺, Ni⁴⁺, Co⁴⁺, and Mn⁴⁺ in sample C and the pristine cathode containing relatively stable TM ions such as Ni²⁺, Co³⁺, and Mn³⁺ were stored with Nitrile electrolyte without additives (1M LiPF₆ in EC/EMC/PN (25/45/30 vol%)). The result showed remarkably similar or even more TM dissolution contents in sample D with a pristine cathode. That is because the highly polar group in PN has strong interaction with TM ions in cathode material to dissolve them out of the cathode making TM-ligand complex in the electrolyte. **(Figure 18)** This explains the contradiction between the stable HOMO energy level of PN itself and low instability towards the cathode material with increasing leakage current in the floating test. Therefore, the cathode protection is necessary for using PN as a low viscosity solvent.

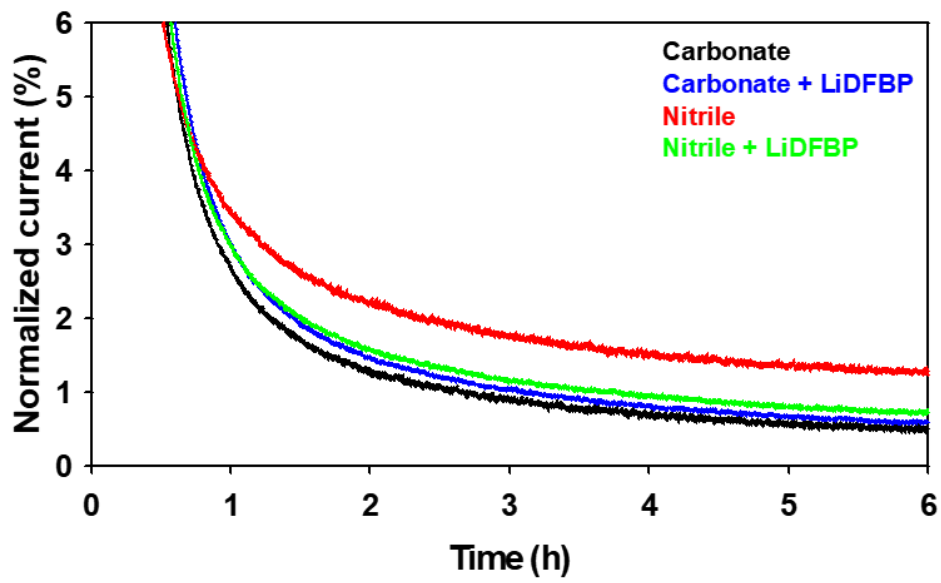


Figure 16. Floating test of NCM/Li half cells charged to 4.3V at C/10 rate and 25oC, magnified to show normalized leakage currents.

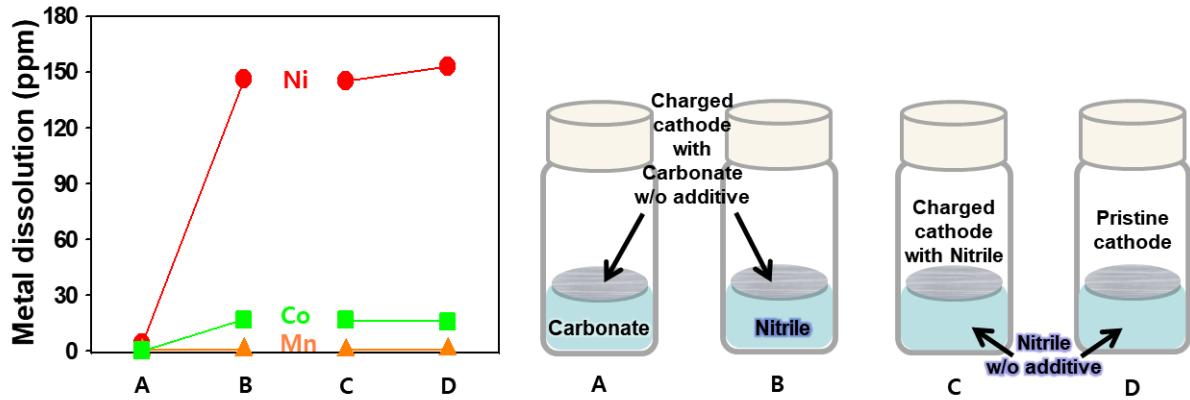


Figure 17. Transition metal dissolution degree analyzed by inductively coupled plasma (ICP). Charged cathodes with Carbonate w/o additive were stored in (a) Carbonate electrolyte and (b) Nitrile electrolyte. (c) Charged cathode with Nitrile and (d) pristine cathode were stored in Nitrile w/o additive.

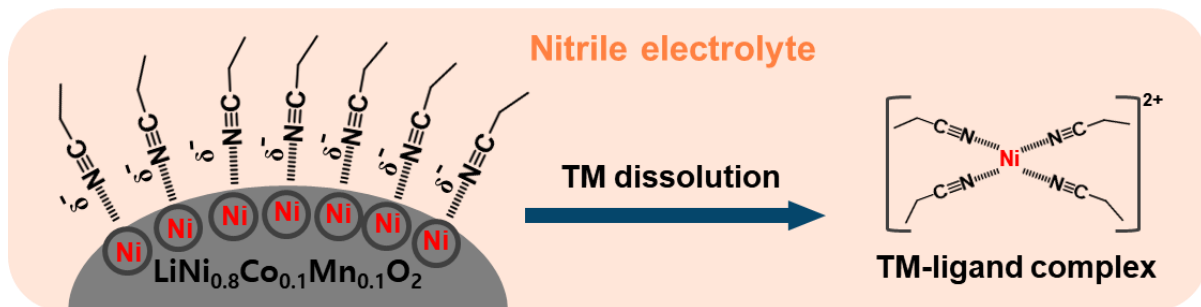


Figure 18. Illustration of TM dissolution of Nitrile out of the NCM cathode.

The oxidation and reduction tendencies of components in the electrolyte can be estimated by calculation of highest occupied molecular orbital (HOMO) energy and lowest unoccupied molecular orbital (LUMO) energy. The higher the HOMO level and the lower the LUMO level, the more possible to be oxidized and reduced, each. Density functional theory (DFT) was used in the calculation of the energy levels of typical components in the electrolyte in **Figure 19**. The FEC additive, famous for its SEI forming ability on the silicon anode [14], [27], would be reduced first at the anode. The LiDFBP additive is expected to reduce after FEC and oxidize faster than the other components like EC and FEC. The HOMO and LUMO level of PN cosolvent are not shown in Fig. , but we can estimate it to be reduced at a similar level of EC (LUMO of EC: -0.35 eV, PN: -0.34 eV) and have high anodic stability (HOMO of EC: -8.60 eV, PN: -9.45 eV) as shown in **Table 1**.

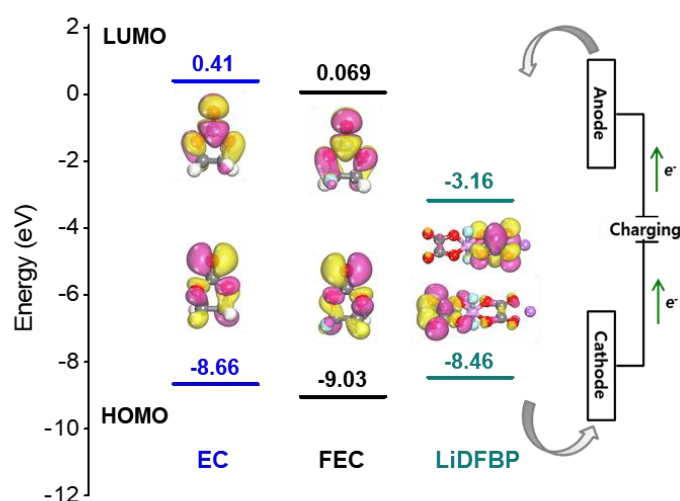


Figure 19. Density functional theory (DFT) calculation of HOMO-LUMO energy level and chemical structures. (EC, FEC, and LiDFBP in neutral charge of the molecule. C, H, O and F atoms are represented in gray, white, red and cyan colored spheres, respectively.)

Based on this oxidation and reduction tendencies, the precycle of NCM/gra-SiC full cell was conducted. **Figure 20(a)** shows the comparison of the voltage profiles of NCM/gra-SiC full cells precycled with and without LiDFBP, and whether PN included or not. The LiDFBP additive revealed slightly increased overpotential when charging, which is expected to be caused by the LiDFBP reduction as shown in **Figure 20(b)**. In contrast, Nitrile + LiDFBP had less polarization thanks to the low viscosity and good impregnation characteristic of .PN. The dQ/dV plot indicates faster kinetics of Nitrile electrolytes relative to the typical electrolyte with carbonate solvents. The improved Li⁺ ion diffusion facilitated by PN leads to the reduction of ohmic polarization by Nitrile. The formation of the LiDFBP-derived SEI layer on the gra-SiC anode can be anticipated in that FEC reduction peak shifts to higher voltages.

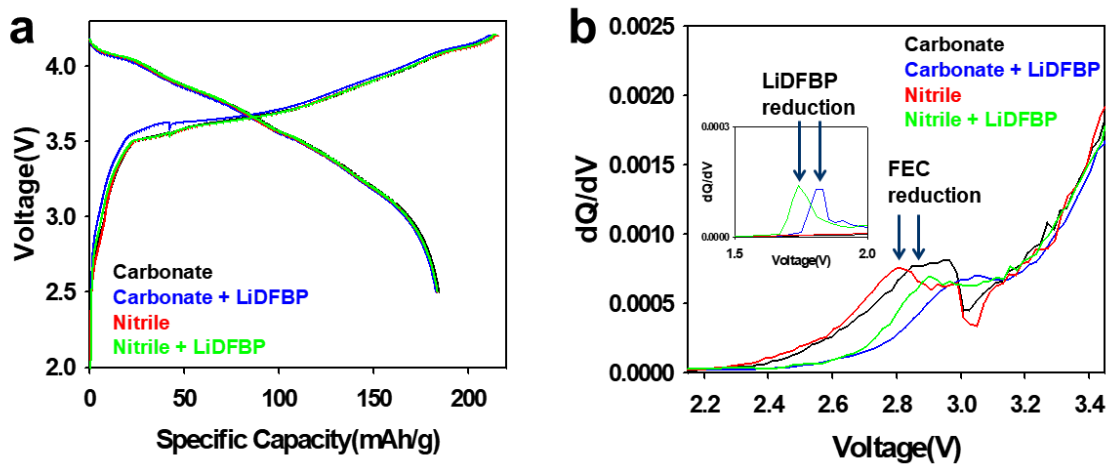


Figure 20. (a) Charge-discharge curves and (b) charge differential capacity (dQ/dV) plots on the NCM/gra-SiC full cells during precycle under C/10 at 25 °C.

The rate capability performance at various discharge current densities shows the positive effect of the propionitrile cosolvent and the LiDFBP additive confirmed in **Figure 21**. The Nitrile electrolyte shows outstanding performance on the rate capability compared to the Carbonate electrolyte, as expected concerning the low viscosity and improved impregnation characteristic. However, the capacity recovery at $C/2$ rate after $2C$ rate cycles experiences degradation resulting from the anodic instability on the NCM cathode, as discussed in the floating test (**Figure 16**). On the other hand, the Nitrile + LiDFBP electrolyte delivers not only an excellent discharge capacity at a high C rate ($2C$, 93 mAh/g, for capacity retention of 53.5% versus $C/5$), but also stable capacity recovery at $C/2$ rate. The LiDFBP-derived SEI layer prevents the deterioration of NCM cathode originated from the oxidation of propionitrile with stable protective film on the cathode. In contrast to the Nitrile and Nitrile + LiDFBP electrolyte, the Carbonate and the Carbonate + LiDFBP displayed inferior rate capability with increasing current density ($2C$, 53.6 mAh/g, and 57.2 mAh/g, corresponding to a capacity retention of 30.7% and 32.9%, respectively) since the carbonate-based electrolyte has low impregnation characteristic on the high-mass-loading electrodes.

Figure 21(b) shows the ac impedance spectra of the NCM cathode/gra-SiC anode full cells after precycle at room temperature, depending on the used electrolytes whether containing the propionitrile cosolvent or not and the LiDFBP additive or not. The LiDFBP additive slightly increased the interfacial resistance involving the SEI resistance and charge transfer resistance because it tends to form an SEI layer on both the surface of the cathode and the anode as expected by HOMO-LUMO energy level calculation. (**Figure 19**) The significant feature is the much smaller semicircle in the full cell EIS with the Nitrile electrolyte than one with the Carbonate electrolyte. This indicates that the low viscosity of the electrolyte using the propionitrile cosolvent exerts a favorable influence upon the lithium-ion transport.

Based on the cycling stability, rate capability and interfacial resistance, the effect of bulk characteristic thanks to propionitrile cosolvent is powerful for the rate capability on the high-mass-loading electrodes, and LiDFBP additive-derived SEI layer can protect electrolyte decomposition on the electrodes, which implies the importance of the bulk characteristics and efficient SEI-layer forming ability of electrolytes.

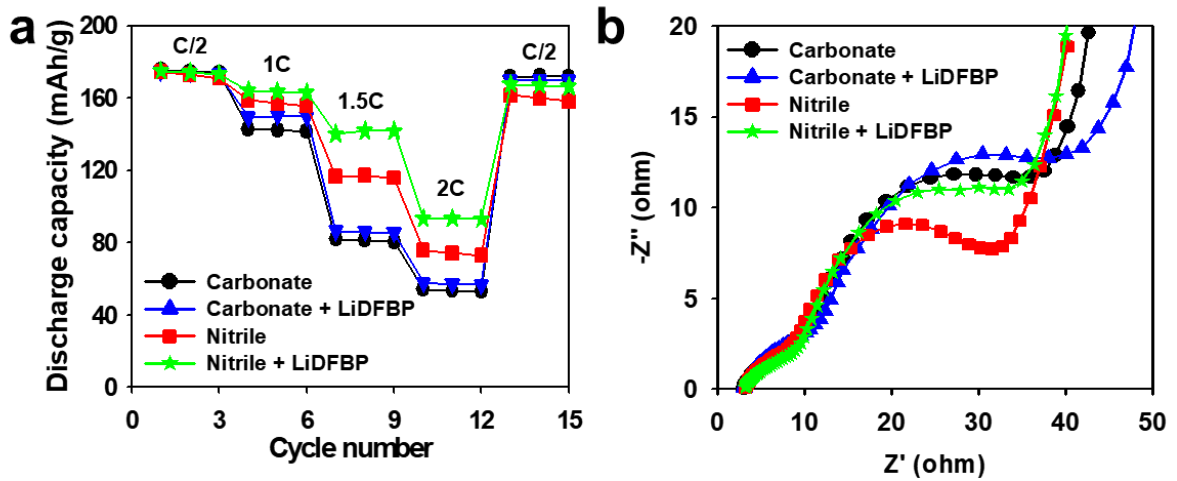
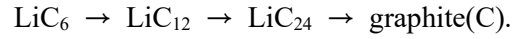


Figure 21. (a) Comparison of the discharge rate capability of NCM/gra-SiC full cells with electrolytes whether containing nitrile cosolvent and LiDFBP additive or not. The discharge rate was from C/2 to 2C with C/2 rate fixed to charge. (b) The AC impedances spectra of NCM/gra-SiC full cells after the precycle.

Figure 22 shows the XRD patterns of the discharged gra-SiC anodes from NCM/gra-SiC full cells with and without PN and LiDFBP in the electrolyte after 2C rate cycles of rate capability test. The trapped lithium ions inside the anode electrodes decrease with the higher rate capability performance of the cells using among four kinds of electrolytes, assuming the delithiation reaction is



The Nitrile electrolyte reveals superior delithiation ability than the Carbonate electrolyte, thanks to its advantageous bulk characteristic on the fast discharging. Furthermore, we can demonstrate that the SEI layer on the gra-SiC anode with decomposed species of LiDFBP has a beneficial effect on Li-ion kinetics through the SEI layer, improving the rate capability.

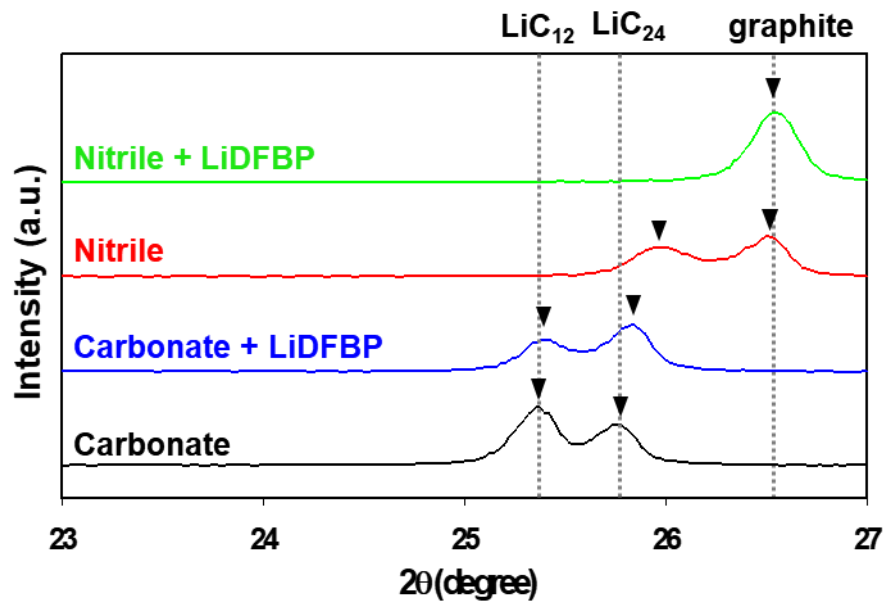


Figure 22. XRD patterns of the gra-SiC anodes in the electrolyte with and without propionitrile and LiDFBP.

The cycling stability and coulombic efficiency of NCM cathode/gra-SiC anode full cells at 45°C are displayed in **Figure 23(a) and (b)**. The Carbonate electrolyte shows the best performance than the others. Contrary to the expectation for the LiDFBP additive, the Carbonate + LiDFBP electrolyte shows slightly decreased capacity retention at the 50th cycle than the Carbonate electrolyte (86.1% for Carbonate and 83.8% for Carbonate + LiDFBP). This result is assumed to the low initial discharge capacity due to the slightly larger interfacial resistance of LiDFBP-containing electrolytes (**Figure 21(b)**).

The cell with the Nitrile electrolyte shows a sharp decline in discharge capacity at the 50th cycle and coulombic efficiency, particularly after 30 cycles. The Nitrile + LiDFBP electrolyte, however, reveals dramatically improved cycling stability and coulombic efficiency. This advanced performance can be a reasonable explanation that the LiDFBP additive can suppress electrolyte decomposition and deterioration of NCM cathode during cycles. Moreover, the LiDFBP additive can prevent the cathode from HF attack, which would lead to LiF compounds growing in the protective film by promoting hydrolysis of LiPF₆ salt.[28] Nevertheless, the cycling instability of the PN cannot be completely overcome by the Nitrile + LiDFBP electrolyte and the discharge capacity retention is relatively lower (78.5% at 50th cycle) than that of the Carbonate electrolyte (86.1% at 50th cycle). This is estimated to the degradation of the electrodes and the additives cannot perfectly prevent the effect of PN on them.

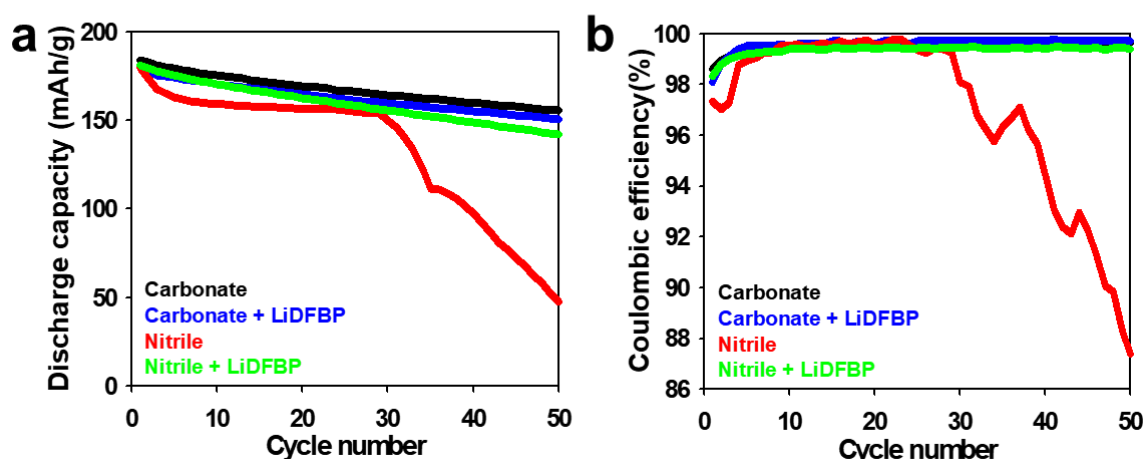


Figure 23. (a) Cycle retention and (b) coulombic efficiency of NCM/gra-SiC full cells in the voltage range 2.5 – 4.2 V at a rate of C/5 at 45 °C.

To confirm whether the Nitrile affects a detrimental reaction on the NCM cathode during cycling, the SEM analysis of the NCM cathodes was performed. **Figure 24** shows the cross-sectional SEM images of uncycled pristine NCM cathode and cycled NCM cathodes retrieved from the cells with the Nitrile and the Nitrile + LiDFBP electrolyte. The pristine NCM consists of large particles and small particles of NCM active materials. They are secondary particles comprised of primary particles assembled. These secondary particles can break off occurring microcracks between primary particles as the NCM structure repeats lithiation-delithiation and volume changes. [6] Already cracked particles near the surface comes from the pressing process during manufacturing the high-mass-loading cathode. [29] The volume expansion is much less in the Nitrile + LiDFBP electrolyte (between 57.47 μm and 62.86 μm) than one in the Nitrile electrolyte (70.42 μm). The cathode cycled with Nitrile electrolyte suffers from microcracks in almost every secondary particle. Unlike the Nitrile, the Nitrile + LiDFBP electrolyte has much less secondary particle breakdown. Furthermore, the byproducts layer on the electrode is much thicker on the Nitrile electrolyte, which can act as a resistive layer, responsible for the irreversible loss of capacity because of the material lost for its formation and also for a significant impedance growth.[30]

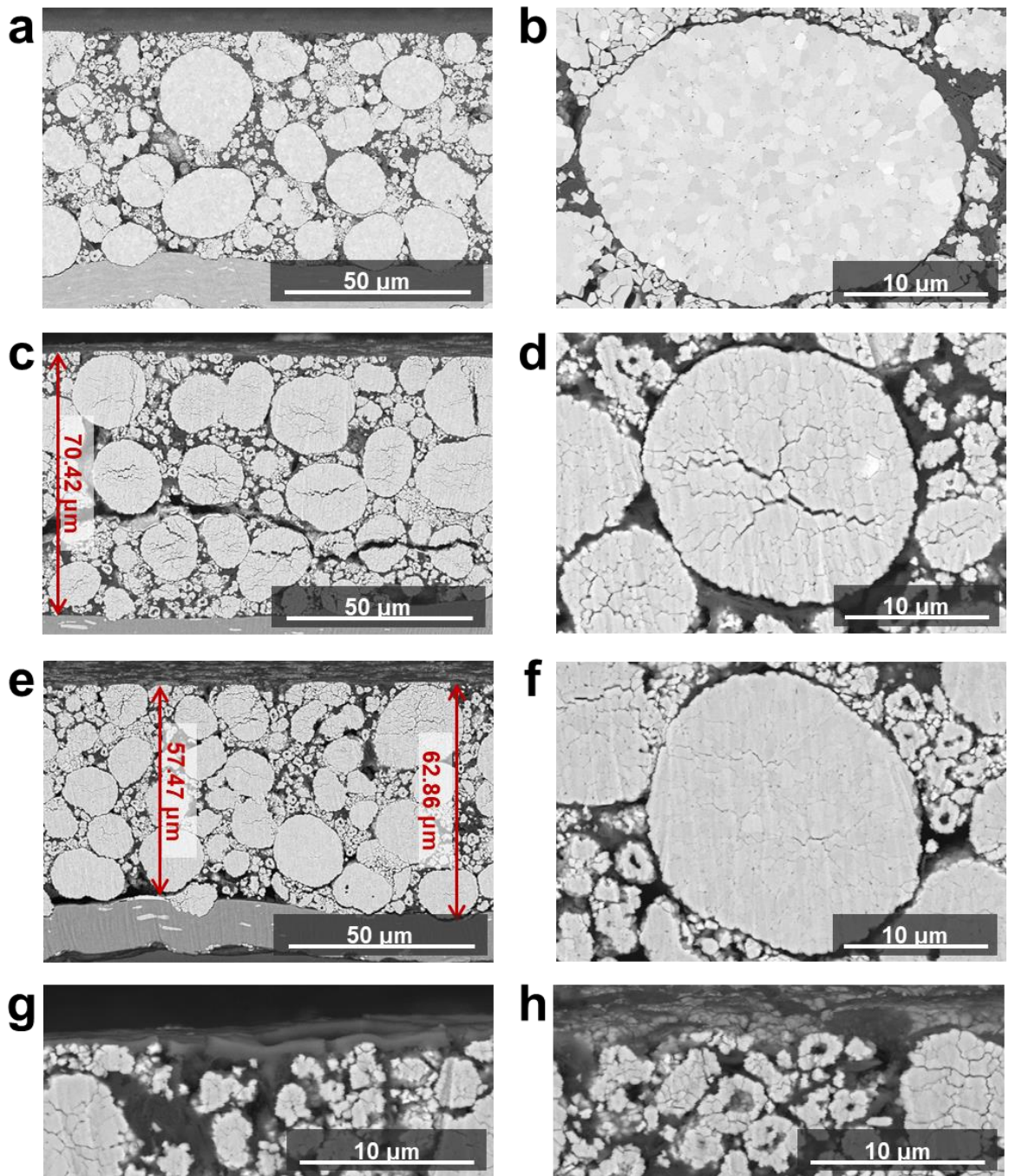


Figure 24. BSE images from the cross-sectional SEM of NCM cathodes (a), (b) pristine, (c), (d), (g) cycled with Nitrile electrolyte, and (e), (f), (h) cycled with Nitrile + LiDFBP electrolyte.

The cross-sectional images of the cycled gra-SiC anode are shown in **Figure 25**. The parted crack in cross-sectional SEM can occur during ion-milling because the active materials grow too weak after cycling to endure the milling force, especially in the case of the high-mass-loading electrodes and highly depleted electrodes. Despite considering the cleavage, the gra-SiC anode cycled with the Nitrile electrolyte expanded much more than the Nitrile + LiDFBP electrolyte (**Figure 25(a)**). Moreover, the SEI layer on the anode is thicker with the Nitrile electrolyte (**Figure 25(b)**). The degree of deterioration of the active materials, however, seems not that different in that the silicon in the SiC particle is expanded to be separated from the graphite. Thus, the low cycle performance of the Nitrile + LiDFBP electrolyte is supposed to result from the degradation of the gra-SiC anodes.

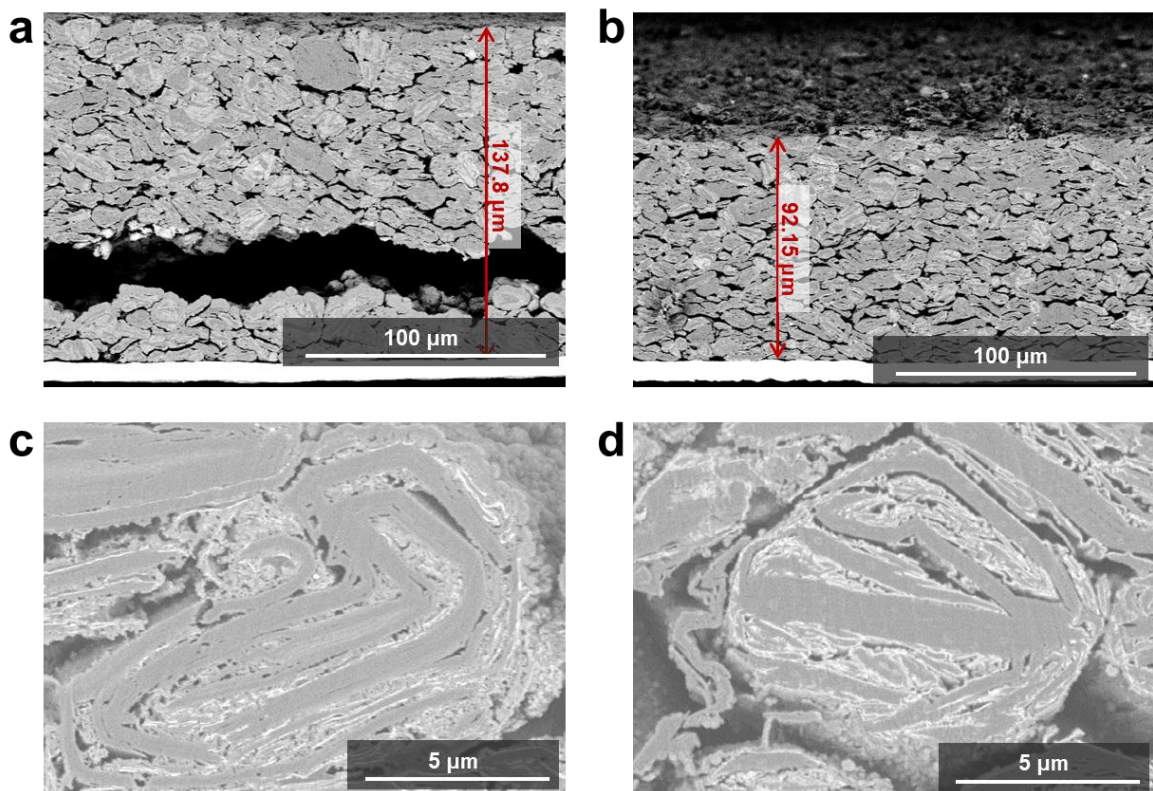


Figure 25. BSE images from the cross-sectional SEM of gra-SiC anodes (a), (c) cycled with Nitrile electrolyte, and (b), (d) cycled with Nitrile + LiDFBP electrolyte.

3.3 Surface Analysis

The effect of electrolyte composition on the NCM cathode surface chemistry is presented in **Figure 26**. First, explaining the Nitrile electrolyte compared to the Carbonate electrolyte, the F 1s spectra (**Figure 26(a), (c), (e)**) acquired on the NCM cathodes after the precycle and further 3 cycles shows a relatively low peak at 687.7 eV, corresponding to the PVdF binders on the cathodes, and no significant difference in the LiF peak at 684.9 eV. The small binder peak is attributed to the formation of thick chemisorbed PN solvent or byproducts by electrolyte decomposition on the cathodes, the components of which can be found on the N 1s spectra exhibiting C≡N compounds at 399.7 eV, and C=N compounds at 398.6 eV. After 50 cycles at elevated temperature (**Figure 26(b), (d), (f)**), we can see almost no binder peak and large signals of C=O-based components (O⁻ peak) in the Nitrile electrolyte. According to Song et al, a polar nitrile moiety can make a balance of the effective charge of a transition metal atom on the cathode surface (a cobalt atom on LiCoO₂ cathode in this study), creating chemisorption layer of (-CN-TM) complexes, which physically expels other components in electrolyte, enhancing the thermal stability. [31] The O 1s spectra after initial cycles show similar results of larger O^{-(1-a)} peak at 533.8 eV of the Nitrile electrolyte than other electrolytes. The reason why the Nitrile + LiDFBP electrolyte has a similar intensity to the carbonate-based electrolyte is that the SEI layer formed by LiDFBP additive prevents the exposure of transition atom on the cathode surface. [31]–[36] (**Figure 27**)

A comparison of the Nitrile electrolyte with the Carbonate electrolyte in **Figure 26(d)** clearly shows that the Nitrile has no effect on diminishing LiF contents acting as the resistive layer on the cathodes but decompose continuously forming C=O-based byproducts on them. The highly different intensity of O⁻ peak between Nitrile and Nitrile + LiDFBP demonstrates the protection of LiDFBP additive on the cathode surface.

The LiDFBP additive has an important bearing on protecting the NCM cathode from the consistent decomposition of PN with developing LiDFBP-derived SEI layer. F 1s spectra show drastically reduced the peak of LiF, indicating that the protective film on the cathode can restrain the oxidation of LiPF₆ salt leading to the formation of resistive LiF, as reported by Choi. et al. [16] The low amounts of LiF component would make more ionic conductive SEI layer on the NCM cathode, performing enhanced rate capability (**Figure 21(a)**). The LiDFBP additive also affects to diminish electrolyte decomposition like C=O compounds. Thanks to the surface protective film based on the LiDFBP-derived SEI, the Nitrile + LiDFBP electrolyte seem to alleviate the oxidation of PN, leading to enormously improved cycle stability (**Figure 23(a)**).

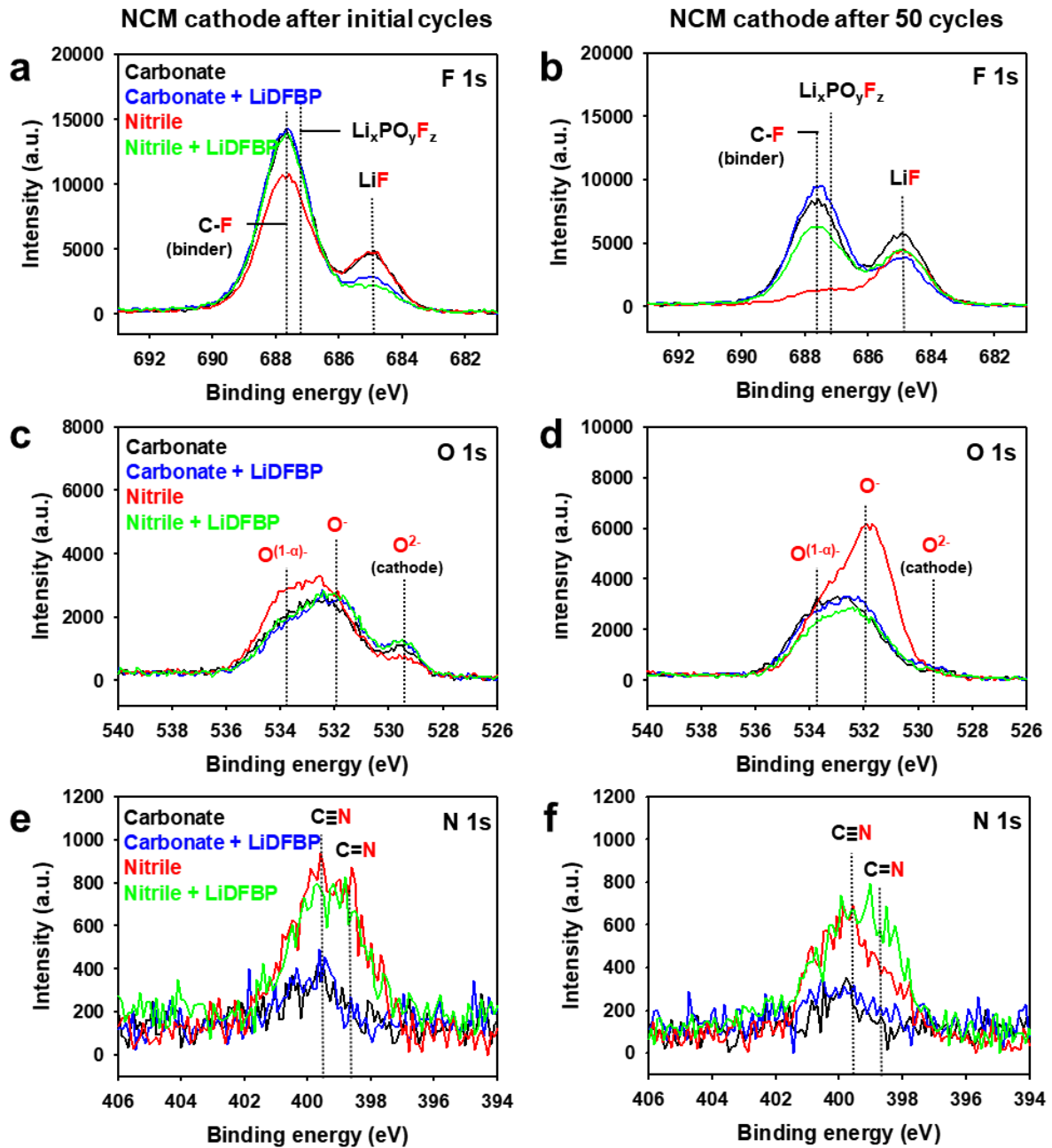


Figure 26. F 1s, O 1s and N 1s XPS spectra of the NCM cathodes retrieved from NCM/gra-SiC full cells (a), (c), (e) after precycle and (b), (d), (f) after the cycle test.

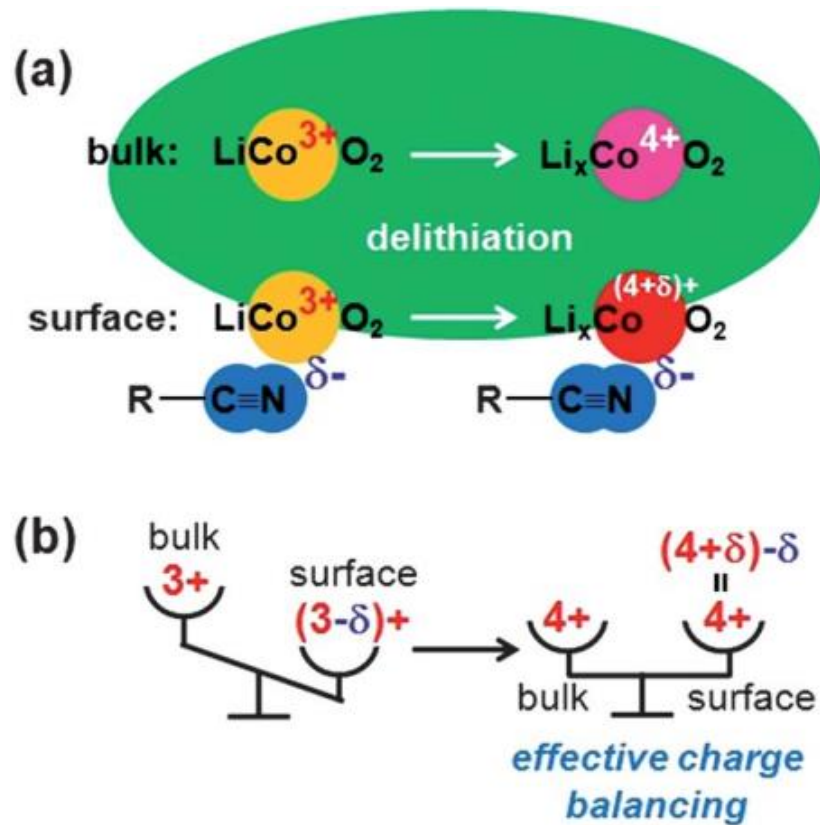


Figure 27. (a) Cobalt atom's charge change depending on the bulk and the surface after delithiation. (b) The effective charge of cobalt versus cobalt-succinonitrile complex depending on in the bulk or at the surface.

Figure 28 shows the F 1s, P 2p, and N 1s XPS spectra for the anodes with and without PN and LiDFBP after precycle and further 3 cycles and after 50 cycles. The peak of the Nitrile electrolyte shows a similar shape of one with the Carbonate electrolyte after initial cycles. However, the noticeable feature for the gra-SiC anode is the appearance of LiF at 684.9 eV and NiF₂ at 687.3 eV on F 1s by both the Carbonate and the Nitrile electrolyte, and C≡N at 399.7 eV and C=N at 398.6 eV on N 1s spectra by the Nitrile and the Nitrile + LiDFBP electrolyte after cycle test of 50 cycles at C/2 rate and 45°C. The uncontrollable decomposition of the PN cosolvent seems to cause the formation of an N-based SEI layer, which aggravates the cycle retention (**Figure 23(a)**). A relatively high amount of LiF does not seem to influence on the discharge capacity degradation during the cycle test since the Carbonate shows similar peak intensity, displaying the superior cycle performance.

As presented on the F 1s and P 2p spectra, the SEI layer derived by the Carbonate + LiDFBP electrolyte after initial cycles consist of a large amount of LiF, forming a rigid SEI layer and suppressing further electrolyte decomposition, but also leading to high interfacial resistance (**Figure 21(b)**). The increased LiF peaks of the Carbonate + LiDFBP, Nitrile, and Nitrile + LiDFBP electrolytes on the cycled gra-SiC anode results from the consistent decomposition of electrolytes. The LiDFBP containing electrolyte such as Carbonate + LiDFBP and Nitrile + LiDFBP presents a new peak at 134.5 eV and 133.4 eV on P 2p spectra, corresponding to the ionic conductive P-O component in the LiDFBP-derived SEI layer, which is beneficial for the rate capability (**Figure 21(a)**). However, the peak size of the P-O component of the Nitrile + LiDFBP is smaller than one of the Carbonate + LiDFBP, though they both contain the same weight percent of the LiDFBP additive. Besides, the peak at 687.3 eV indicating Li_xPO_yF_x peak at 687.3 eV and LiF peak at 684.9 eV show no significant difference with the Nitrile electrolyte without LiDFBP. It would be the effect of PN covering by N-based reduction products after the reductive decomposition of LiDFBP on the gra-SiC anodes. The increased peaks of C≡N and C=N on N 1s after cycle test would be the reason for the degradation of discharge capacity retention of Nitrile and Nitrile + LiDFBP electrolytes.

Therefore, PN cosolvent and LiDFBP additive decompose at both electrodes, forming the SEI layer, and affect the electrochemical performances.

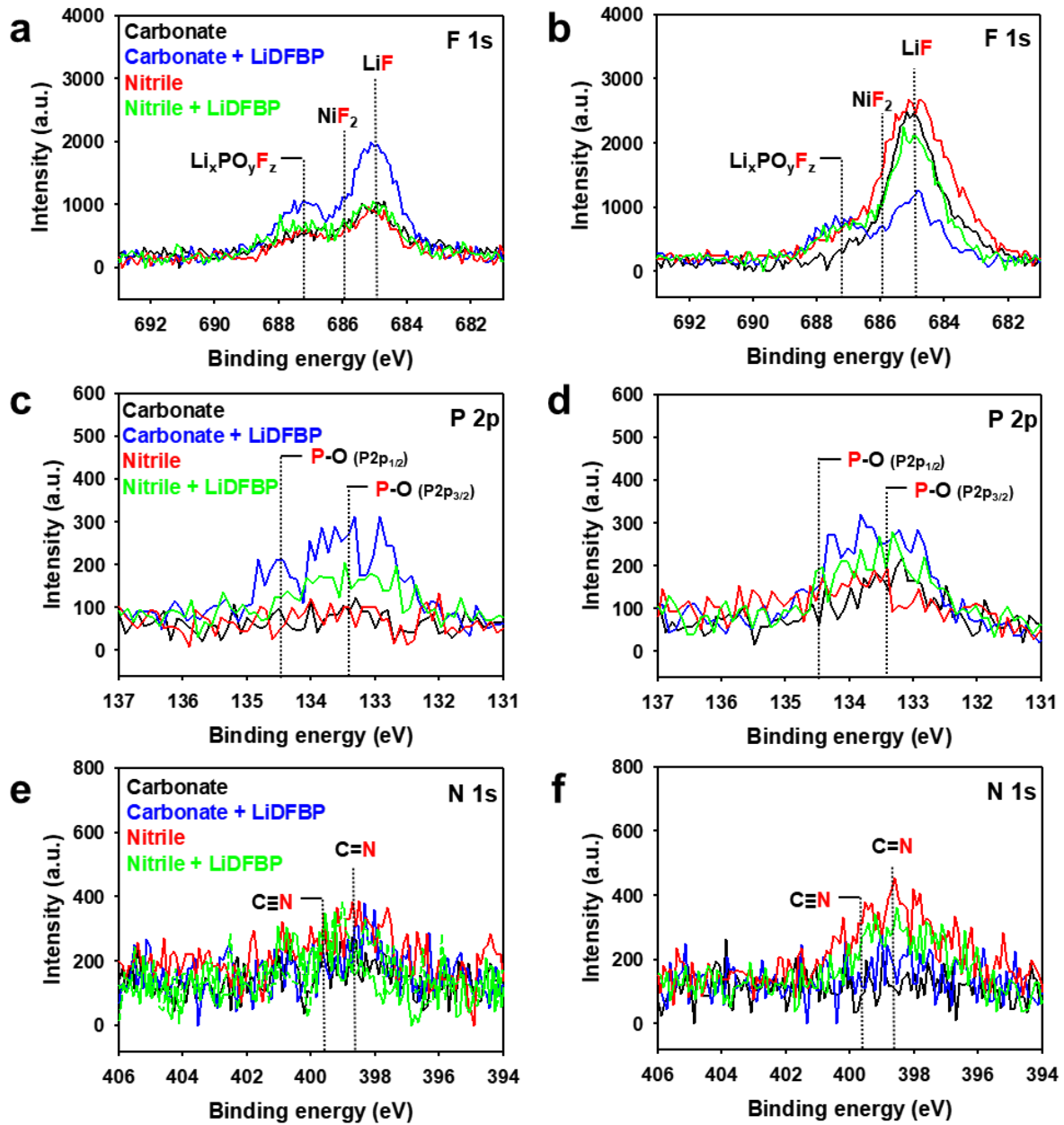


Figure 28. F 1s, P 2p, and N 1s XPS spectra of gra-SiC anodes from NCM/gra-SiC full cells (a), (c), (e) after precycle at C/10 and 3 cycles at C/2 and 25°C, and (b), (d), (f) after 50 cycles at C/2 and 45°C.

4. Conclusion

In this study, we investigated the effect of PN cosolvent and LiDFBP additive on the improvement of dischargeability to enable fast discharging. PN cosolvent mainly contributes to fast lithium-ion transport in the bulk electrolyte with advantages of low viscosity and outstanding impregnation characteristic. In addition, the LiDFBP-derived SEI layer consists of ionic conductive P-O based and lithium ion-containing components, which induces a high rate of lithium-ion passing through the SEI layers. The superior bulk characteristic and the ionic conductive protective film demonstrate their important role in the enhancement of discharge rate capability. However, the PN seems to be decomposed at both electrodes, deteriorating them during cycle tests. The problem could be almost solved by introducing LiDFBP additive to protect the electrode especially the NCM cathode from the continuous decomposition of the electrolyte.

5. Reference

- [1] Y. Nishi, “Lithium ion secondary batteries; past 10 years and the future,” 2001.
- [2] M. M. Thackeray, C. Wolverton, and E. D. Isaacs, “Electrical energy storage for transportation—approaching the limits of, and going beyond, lithium-ion batteries,” *Energy Environ. Sci.*, vol. 5, pp. 7854–7863, 2012.
- [3] B. Scrosati and J. Garche, “Lithium batteries: Status, prospects and future,” *J. Power Sources*, vol. 195, pp. 2419–2430, 2010.
- [4] D. V Pelegov and J. Pontes, “Main Drivers of Battery Industry Changes: Electric Vehicles-A Market Overview,” *Batteries*, vol. 4, no. 65, p. 1, 2018.
- [5] A. M. Haregewoin, A. S. Wotango, and B.-J. Hwang, “Electrolyte additives for lithium ion battery electrodes: progress and perspectives,” *Energy Environ. Sci.*, vol. 9, pp. 1955–1988, 2016.
- [6] F. Schipper, E. M. Erickson, C. Erk, J. Y. Shin, F. F. Chesneau, and D. Aurbach, “Review—Recent advances and remaining challenges for lithium ion battery cathodes I. Nickel-rich, $\text{LiNi}_x\text{Co}_y\text{Mn}_z\text{O}_2$,” *J. Electrochem. Soc.*, vol. 164, no. 1, pp. A6220–A6228, 2017.
- [7] Y. Jin, B. Zhu, Z. Lu, N. Liu, and J. Zhu, “Challenges and recent progress in the development of Si anodes for lithium-ion battery,” *Adv. Energy Mater.*, vol. 7, no. 23, pp. 1–17, 2017.
- [8] H. Wu and Y. Cui, “Designing nanostructured Si anodes for high energy,” *Nano Today*, vol. 7, pp. 414–429, 2012.
- [9] Z. Du, D. L. Wood, C. Daniel, S. Kalnaus, and J. Li, “Understanding limiting factors in thick electrode performance as applied to high energy density Li-ion batteries,” *J. Appl. Electrochem.*, vol. 47, no. 3, pp. 405–415, 2017.
- [10] H. Zheng, J. Li, X. Song, G. Liu, and V. S. Battaglia, “A comprehensive understanding of electrode thickness effects on the electrochemical performances of Li-ion battery cathodes,” *Electrochim. Acta*, vol. 71, pp. 258–265, 2012.
- [11] D. Y. W. Yu, K. Donoue, T. Inoue, M. Fujimoto, and S. Fujitani, “Effect of electrode parameters on LiFePO_4 cathodes,” *J. Electrochem. Soc.*, vol. 153, no. 5, pp. 4–8, 2006.
- [12] K. G. Gallagher *et al.*, “Optimizing areal capacities through understanding the limitations of lithium-ion electrodes,” *J. Electrochem. Soc.*, vol. 163, no. 2, pp. A138–A149, 2016.
- [13] C. K. Kim *et al.*, “Synergistic Effect of Partially Fluorinated Ether and Fluoroethylene Carbonate for High-Voltage Lithium-Ion Batteries with Rapid Chargeability and Dischargeability,” *ACS Appl. Mater. Interfaces*, vol. 9, no. 50, pp. 44161–44172, 2017.
- [14] N. S. Choi, K. H. Yew, K. Y. Lee, M. Sung, H. Kim, and S. S. Kim, “Effect of fluoroethylene carbonate additive on interfacial properties of silicon thin-film electrode,” *J. Power Sources*,

- vol. 161, no. 2, pp. 1254–1259, 2006.
- [15] T. Jaumann *et al.*, “Lifetime vs. rate capability: Understanding the role of FEC and VC in high-energy Li-ion batteries with nano-silicon anodes,” *Energy Storage Mater.*, vol. 6, no. August 2016, pp. 26–35, 2017.
- [16] J. G. Han *et al.*, “Interfacial Architectures Derived by Lithium Difluoro(bisoxalato) Phosphate for Lithium-Rich Cathodes with Superior Cycling Stability and Rate Capability,” *ChemElectroChem*, vol. 4, no. 1, pp. 56–65, 2017.
- [17] H. Bin Son *et al.*, “Effect of reductive cyclic carbonate additives and linear carbonate co-solvents on fast chargeability of LiNi_{0.6}Co_{0.2}Mn_{0.2}O₂/graphite cells,” *J. Power Sources*, vol. 400, no. May, pp. 147–156, 2018.
- [18] O. Matsuoka *et al.*, “Ultra-thin passivating film induced by vinylene carbonate on highly oriented pyrolytic graphite negative electrode in lithium-ion cell,” *J. Power Sources*, vol. 108, no. 1–2, pp. 128–138, 2002.
- [19] C. C. Chang, S. H. Hsu, Y. F. Jung, and C. H. Yang, “Vinylene carbonate and vinylene trithiocarbonate as electrolyte additives for lithium ion battery,” *J. Power Sources*, vol. 196, no. 22, pp. 9605–9611, 2011.
- [20] L. Chen, K. Wang, X. Xie, and J. Xie, “Effect of vinylene carbonate (VC) as electrolyte additive on electrochemical performance of Si film anode for lithium ion batteries,” *J. Power Sources*, vol. 174, no. 2, pp. 538–543, 2007.
- [21] J. Arai, “Nonflammable methyl nonafluorobutyl ether for electrolyte used in lithium secondary batteries,” *J. Electrochem. Soc.*, vol. 150, no. 2, pp. 219–228, 2003.
- [22] K. Naoi, E. Iwama, N. Ogihara, Y. Nakamura, H. Segawa, and Y. Ino, “Nonflammable hydrofluoroether for lithium-ion batteries: Enhanced rate capability, cyclability, and low-temperature performance,” *J. Electrochem. Soc.*, vol. 156, no. 4, pp. 272–276, 2009.
- [23] R. Marom, O. Haik, D. Aurbach, and I. C. Halalay, “Revisiting LiClO₄ as an electrolyte for rechargeable lithium-ion batteries,” *J. Electrochem. Soc.*, vol. 157, no. 8, pp. 972–983, 2010.
- [24] M. Xu, L. Hao, Y. Liu, W. Li, L. Xing, and B. Li, “Experimental and theoretical investigations of dimethylacetamide (DMAc) as electrolyte stabilizing additive for lithium ion batteries,” *J. Phys. Chem. C*, vol. 115, no. 13, pp. 6085–6094, 2011.
- [25] S. J. An, J. Li, C. Daniel, D. Mohanty, S. Nagpure, and D. L. Wood, “The state of understanding of the lithium-ion-battery graphite solid electrolyte interphase (SEI) and its relationship to formation cycling,” *Carbon N. Y.*, vol. 105, pp. 52–76, 2016.
- [26] R. Wagner *et al.*, “Impact of Selected LiPF₆ Hydrolysis Products on the High Voltage Stability of Lithium-Ion Battery Cells,” *ACS Appl. Mater. Interfaces*, vol. 8, no. 45, pp. 30871–30878, 2016.
- [27] J. S. Kim, D. Byun, and J. K. Lee, “Electrochemical characteristics of amorphous silicon thin

- film electrode with fluoroethylene carbonate additive,” *Curr. Appl. Phys.*, vol. 14, no. 4, pp. 596–602, 2014.
- [28] D. Aurbach *et al.*, “Study of surface phenomena related to electrochemical lithium intercalation into Li_xMO_y host materials ($M = \text{Ni}, \text{Mn}$),” *J. Electrochem. Soc.*, vol. 147, no. 4, pp. 1322–1331, 2000.
- [29] B. S. Lee *et al.*, “Analysis of rate-limiting factors in thick electrodes for electric vehicle applications,” *J. Electrochem. Soc.*, vol. 165, no. 3, pp. A525–A533, 2018.
- [30] F. Friedrich *et al.*, “Editors’ Choice—Capacity Fading Mechanisms of NCM-811 Cathodes in Lithium-Ion Batteries Studied by X-ray Diffraction and Other Diagnostics,” *J. Electrochem. Soc.*, vol. 166, no. 15, pp. A3760–A3774, 2019.
- [31] Y. S. Kim, T. H. Kim, H. Lee, and H. K. Song, “Electronegativity-induced enhancement of thermal stability by succinonitrile as an additive for Li ion batteries,” *Energy Environ. Sci.*, vol. 4, no. 10, pp. 4038–4045, 2011.
- [32] Y. Ji, Z. Zhang, M. Gao, Y. Li, M. J. McDonald, and Y. Yang, “Electrochemical behavior of suberonitrile as a high-potential electrolyte additive and Co-solvent for $\text{Li}[\text{Li}_{0.2}\text{Mn}_{0.56}\text{Ni}_{0.16}\text{Co}_{0.08}]\text{O}_2$ cathode material,” *J. Electrochem. Soc.*, vol. 162, no. 4, pp. A774–A780, 2015.
- [33] Y. Ji *et al.*, “Synergistic effects of suberonitrile-LiBOB binary additives on the electrochemical performance of high-voltage LiCoO_2 electrodes,” *J. Electrochem. Soc.*, vol. 162, no. 13, pp. A7015–A7023, 2015.
- [34] Y. S. Kim, H. Lee, and H. K. Song, “Surface complex formation between aliphatic nitrile molecules and transition metal atoms for thermally stable lithium-ion batteries,” *ACS Appl. Mater. Interfaces*, vol. 6, no. 11, pp. 8913–8920, 2014.
- [35] Y. Abu-Lebdeh and I. Davidson, “New electrolytes based on glutaronitrile for high energy/power Li-ion batteries,” *J. Power Sources*, vol. 189, no. 1, pp. 576–579, 2009.
- [36] Y. Abu-Lebdeh and I. Davidson, “High-voltage electrolytes based on adiponitrile for Li-ion batteries,” *J. Electrochem. Soc.*, vol. 156, no. 1, pp. 60–65, 2009.